New bimetallic dicyanidoargentate(I)-based coordination compounds: Synthesis, characterization, biological activities and DNA-BSA binding affinities

Nesrin Korkmaz, Ali Aydın, Ahmet Karadağ, Yusuf Yanar, Yelis Maaşoğlu, Ertan Şahin, Şaban Tekin

PII: S1386-1425(16)30620-5
DOI: doi: 10.1016/j.saa.2016.10.035
Reference: SAA 14734

To appear in:

Received date: 17 June 2016
Revised date: 30 September 2016
Accepted date: 20 October 2016

Please cite this article as: Nesrin Korkmaz, Ali Aydın, Ahmet Karadağ, Yusuf Yanar, Yelis Maaşoğlu, Ertan Şahin, Şaban Tekin, New bimetallic dicyanidoargentate(I)-based coordination compounds: Synthesis, characterization, biological activities and DNA-BSA binding affinities, (2016), doi: 10.1016/j.saa.2016.10.035

New Bimetallic Dicyanidoargentate(I)-Based Coordination Compounds: Synthesis, Characterization, Biological Activities and DNA-BSA Binding Affinities

Nesrin Korkmaz[a], Ali Aydın[b], Ahmet Karadağ[a*], Yusuf Yanar[c], Yelis Maaşoğlu[d], Ertan Şahin[e], Şaban Tekin[b]

[a]*Department of Chemistry, College of Arts and Science, Gaziosmanpaşa University, 60250, Tokat, Turkey*
[b]*Department of Molecular Biology and Genetics, Gaziosmanpaşa University, 60250, Tokat, Turkey*
[c]*Department of Plant Protection, Faculty of Agriculture, Gaziosmanpaşa University, 60250, Tokat, Turkey*
[d]*Department of Biotechnology, Çukurova University, 01330, Adana, Turkey*
[e]*Department of Chemistry, Faculty of Science, Atatürk University, 25240, Erzurum, Turkey*

***Corresponding authors:** Ahmet Karadağ, Department of Chemistry, Science and Arts Faculty, Gaziosmanpasa University, Tokat, Turkey

Postal Code: 60250
Tel: 90-356-2521616
Fax: 90-356-2521585

E-mail: *ahmet.karadag@gop.edu.tr*

Running Head: Biological capacities of dicyanidoargentate(I)-based complexes

ABSTRACT

Four compounds -two (**2** and **3**) completely new- of composition [Ni(e*dbea*)$Ag_3(CN)_5$] (**1**), [Cu(e*dbea*)$Ag_2(CN)_4$].H_2O (**2**), [Cd(e*dbea*)$Ag_3(CN)_5$].H_2O (**3**) and [Cd(*edbea*)$_2$] [$Ag(CN)_2$]$_2$.H_2O (**4**) {*edbea*; 2,2'-(ethylenedioxy)bis (ethylamine)}, were synthesized and characterized using elemental, FT-IR, X-Ray (**4**), thermal, variable temperature magnetic measurement (**1** and **2**) and biological techniques. The DNA/BSA binding affinities of **2** and **3** were evaluated by UV-Vis spectrophotometric titrations, ethidium bromide exchange experiments and electrophoretic mobility measurements. Compounds **1** and **4** have previously been characterized and shown to reduce the proliferation and migration of tumor cells. For the sake of clarity, **1** precise mechanism of action on microbial organisms and temperature magnetic measurement were determined. The crystallographic analyses showed that **4** was built up of [Cd(*edbea*)$_2$]^{II} cations and [$Ag_2(CN)_4$]^{II} anions. Complexes demonstrated a remarkable antibacterial (**1-4**), antifungal (**1-4**) and antiproliferative activities (**2** and **3**) to ten human bacterial pathogens, four plant pathogenic fungi or three tumor cells (HeLa, HT29, and C6), respectively. Therefore, our results strongly confirm that cell proliferation, cell morphology, Bcl-2, P53 changes and apoptosis can be related to the pharmacological effects of the complexes as suitable candidate for clinical trials.

Keywords: Dicyanidoargentat(I), 2,2′-(ethylenedioxy)bis(ethylamine), Anticancer activity, Antimicrobial activity, Antifugal activity, Apoptosis

Abbreviations: Bcl-2, B-cell lymphoma 2; CC1, cell conditioning 1; CK7, Cytokeratin 7; CK20, Cytokeratin 20; CPT, camptothecin; HIER, heat-induced epitope retrieval; IC50, the half maximal inhibitory concentration; IHC, immunohistochemistry; LDH, lactate dehydrogenase; P53, tumor protein P53;

1. Introduction

Current studies have focused on improving of new chemotherapeutic agents to be used for therapy of disease without side effects. However, most patients relapse following an initial response to chemotherapy due to drug resistance, side effects, and other obscure reasons. Therefore, the new approach to address these drawbacks has a special importance for the patient. In this field, metal complexes have a promising alternative property for older chemotherapeutic agents, and also some of them have been approved as an antimicrobial (silver), antifungal (manganese) or anticancer (platinum) drugs [1]. Recently, many silver compounds with different pharmacological activity and with outstanding anticancer activity have been reported. For instance, silver coumarin complexes or silver carboxylate dimers exhibited anticancer activity against some of the common types of human carcinoma cells [2, 3]. Also, silver phosphine complexes have anticancer potential especially against *cis*platin resistant cells [4]. Heterocyclic thioamide 2-mercapto-3,4,5,6-tetrahydropyrimidine Ag^{I} complexes and $[SnMe_3(bpe)][Ag(CN)_2].2H_2O$ (bpe: 1,2-bis(4-pyridyl)ethane) displayed vigorous anticancer activity to some types of cancer [5, 6].

The chemistry of cyanido-bridged coordination polymers currently attracts many researcher interests resulting from its own internal complexity as well as significant structural diversity. Generally, these materials have been prepared using heptacyanidometallates $[M(CN)_7]^{4-}$ [7-9], hexacyanidometallates $[M(CN)_6]^{3-}$ [10-12] , tetracyanidometallates $[M(CN)_4]^{2-}$, [10,11, 13,14] and dicyanidometallates $[Ag(CN)_2]^{-}$ or $[Au(CN)_2]^{-}$ [11, 15-17], as building units in bridge with a complex cation. The $[Ag(CN)_2]^{-}$ can act as, a rod ligand forming different spatial structures by establishing a link between two coordination centers [18, 19], as an unidentate ligand impeding certain coordination sites of the M^{II} [20, 21], or as a discrete anion with space filler feature [22, 23]. Moreover, this anion can also produce polymeric structures via Ag….Ag interactions [11, 24-26].

Edbea [2,2′-(ethylenedioxy)bis(ethylamine)] used in this study as a linker is an organic ligand which have two *N*- and two *O*- donor atoms. Because of donor sites, this ligand behaves as a multidantate ligand. According to the literature review *edbea* is only coordinated to the central atom with all donor sites [27, 28]. Şenocak et. al observed cyanido and *edbea* linked *2D* polymeric chain structure in which Ni^{II} is coordinated by four cyanido ligands while Cu^{II} is coordinated by two *edbea* ligands and two cyanido ligands, building up a two dimensional coordination polymer chain [29].

Herein, we reported the preparation and characterization of polymeric [Cu(*edbea*)$Ag_2(CN)_4$].H_2O (**2**), [Cd(*edbea*)$Ag_3(CN)_5$].H_2O (**3**) (*The patented compound at the National level*; **Patent Number**: TR 2012 08885 B) and molecular [Cd(*edbea*)$_2$] [$Ag(CN)_2]_2$.H_2O (**4**), which is determined also using *XRD* technique. In addition, magnetic properties of **1** and **2** were studied in the temperature range of 15-300 K. Antibacterial (**1-4**) and antifungal (**1-4**) activity tests were performed on these cyanido complexes for the first time. Moreover, anticancer and cytotoxic activities of two newly synthesized (**2** and **3**) cyanido complexes were investigated on various cancer cell lines *in vitro* using cell elisa proliferation assay and cell cytotoxicity assays. The mechanism of new coordination polymers action was determined using DNA laddering, TUNEL assays and Bcl-2, P53, CK7, and CK20 intracellular proteins staining. The effects of the novel polymers on Topoisomerase I activity, cell migration and cell morphology were also tested. This paper shows that these polymers with low cytotoxicity were highly antiproliferative action via altering Bcl-2 or P53 levels, suppressing topoisomerase I activity and cell migration process, and they have significant antimicrobial or antifungal action.

2. RESULTS and DISCUSSION

Hereinafter, the results of IR spectra (**1-4**), X-ray analysis (**4**), EPR spectrum (**2**), magnetic properties (**1** and **2)**, anticancer, cytotoxic and DNA/BSA binding analyses (**2** and **3**), antibacterial (**1-4**) and antifungal (**1-4**) tests are reported.

A general description of the IR spectra (Fig S1) and thermal curves (TG and DTG) (Fig S2 and S3) for **1-4** and thermoanalytical data (**2-4**) (Table S1) are given as Supplementary data. All complexes exhibited an identical decomposition behavior. The first process in the thermal decompositions of (**2** and **4**) was dehydration. Then, the neutral *edbea* was liberated from the structure followed by the release of the cyanido groups. While the decomposition product is admixture of metals (Ni + Ag, Cu + Ag and 0.4 Cd + Ag) for complexes **2** and **3**, only Ag metal is found for complex **4** resulting from substantially low boiling point of Cd. Estimated thermal decomposition scheme for **2-4** may be represented as Scheme S1; Supplementary data.

2.1. Structure Description

The structures of **2** and **3** that were not suitable crystals and could not be determined using *XRD* technique. The literature knowledge about the *edbea* ligand [29-31] and the elemental, IR and thermal measurement results reveal that the closed formulas of **2** and **3** should be [Cu(*edbea*)$Ag_2(CN)_4$].H_2O and [Cd(*edbea*)$Ag_3(CN)_5$].H_2O, respectively.

According to *XRD* analysis, **4** has an ionic structure consisting of $[Cd(edbea)_2]^{II}$ cation and $[Ag_2(CN)_4]^{II}$ anion (Figure 1). Each Cd^{II} ion is eight coordinated through four oxygens and four nitrogen atoms from both *edbea* ligands. This ligand uses all of its donor atoms in this compound. Ag^{I} exhibits linear coordination geometry rather than T shaped geometry according to the linear Ag-C-N bond angles while Ag…Ag argentophilic interactions affect significantly the packing forces of the network structure. The Ag–Ag distance of the dimeric fragments, (3.112(13) Å), is below the sum of the van der Walls radii of two silver atoms (3.44 Å) [32]. The short Ag…Ag argentophilic interactions (Ag1…Ag2=3.112(13) Å) is a characteristic of the silver compounds [33, 34] and they contribute to the packing forces of the crystal structure.

Significant bond angles and lengths of **4** are given in Table 1.

Table 1. Selected bond lengths (Å) and angles (°) of **4**

Bond Lengths (Å)			
Cd1 - N3	2,335(5)	Ag1 - C14	2,049(8)
Cd1 - N5	2,340(5)	Ag1 - Ag2	3,112(13)
Cd1 - N6	2,355(5)	Ag2 - C16	2,047(9)
Cd1 - N4	2,361(5)	Ag2 - C15	2,037(9)
Cd1- O1	2,775(7)	C15 - N8	1,123(9)
Cd1 - O2	2,584(4)	N2 - C13	1,135(9)
Cd1 - O3	2,580(4)	N7 - C16	1,141(10)
Cd1 - O4	2,622(4)	N1 - C14	1,111(9)
Ag1 - C13	2,043(9)		
Bond Angles (°)			
N3 - Cd1 - N5	94,8(2)	N3 - Cd1- O4	127,71(17)
N3 - Cd1- N6	91,3(2)	N5 - Cd1- O4	90,36(17)
N5 - Cd1- N6	168,83(19)	N6 - Cd1- O4	78,51(16)
N3 - Cd1- N4	164,02(19)	N4 - Cd1- O4	68,17(16)
N5 - Cd1- N4	86,12(19)	O3 - Cd1 - O4	61,97(14)
N6 - Cd1- N4	90,53(19)	O2 - Cd1 - O4	132,90(14)
N3 - Cd1- O3	68,62(18)	C13 - Ag1 - C14	178,5(3)
N5 - Cd1- O3	77,32(18)	C13 - Ag1 - Ag2	89,2(2)
N6 - Cd1- O3	96,36(18)	C14 - Ag1 - Ag2	92,0(2)
N4 - Cd1- O3	126,90(17)	C15 - Ag2 - C16	175,9(4)
N3 - Cd1- O2	86,34(18)	C16 - Ag2 - Ag1	91,5(3)
N5 - Cd1- O2	121,60(17)	C15 - Ag2 - Ag1	86,2(2)
N6 - Cd1- O2	68,05(16)	N1- C1 - Ag1	179,1(8)
N4 - Cd1- O2	79,65(16)	N7 - C16 - Ag2	176,8(9)
O3 - Cd1- O2	150,57(16)	N2 - C13 - Ag1	175,1(8)

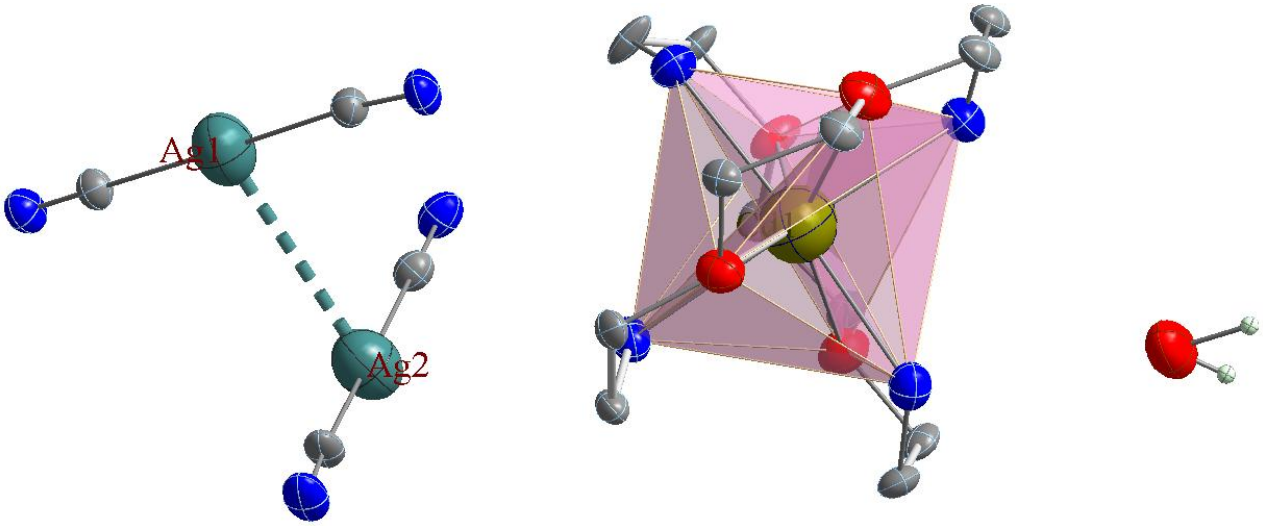

Figure 1. The molecule structure of **4**. H atoms of *edbea* omitted for clarity

Cd^{II} ion in the cation is eight coordinated. Several methods were used to clarify the geometry of eight-coordinated metal centers. Burdett et al. have analyzed eight-coordinated molecules in all possible geometries (dodecahedron, square antiprism, bicapped trigonal prism, cube, hexagonal bipyramid, square prism, bicapped trigonal antiprism) [35]. Muetterties and Wright have reported that the structures with dodecahedron, square antiprism and bicapped trigonal prism geometry have low-energy structures [36]. Haigh has advised a simple criterion for distinguishing the types of low-energy structures. 16th, 17th and 18th lowest LML' angles in Cd^{II} ion are 90.9, 95.5 and 163.5°. Thus we can classify the structure as bicapped trigonal prism. The shape measure suggested by Xu et al using their Matlab® code was also performed [37].

$$S=\min\left[\frac{1}{m}\sqrt{\sum_{i=1}^{m}(\delta_i-\theta_i)^2}\right]$$

Where *m is the* number of edges, δ is an angle between normals of adjacent faces, δ_I is the observed dihedral angle along the *i*th edge of δ, and θ is the same angle of corresponding ideal polytopal shape θ. The smallest *S* value is the one closest to describing the coordination geometry. Atomic coordinates used for shape measure calculation are given in Table S2; Supplementary data.

The shape measure *S* (°) is given below for trigonal dodecahedron (D_{2d}), bicapped trigonal prism (C_{2v}), and square antiprism (D_{4d}):

$S(D_{2d})$= 48.0749°; $S(C_{2V})$= 46.981°; $S(D_{4d})$= 50.1348°

Shape measure results do correlate the result found by Haigh's criteria. The lower shape measure for the bicapped trigonal prism may show that the coordination polyhedron is closest to the bicapped trigonal prism.

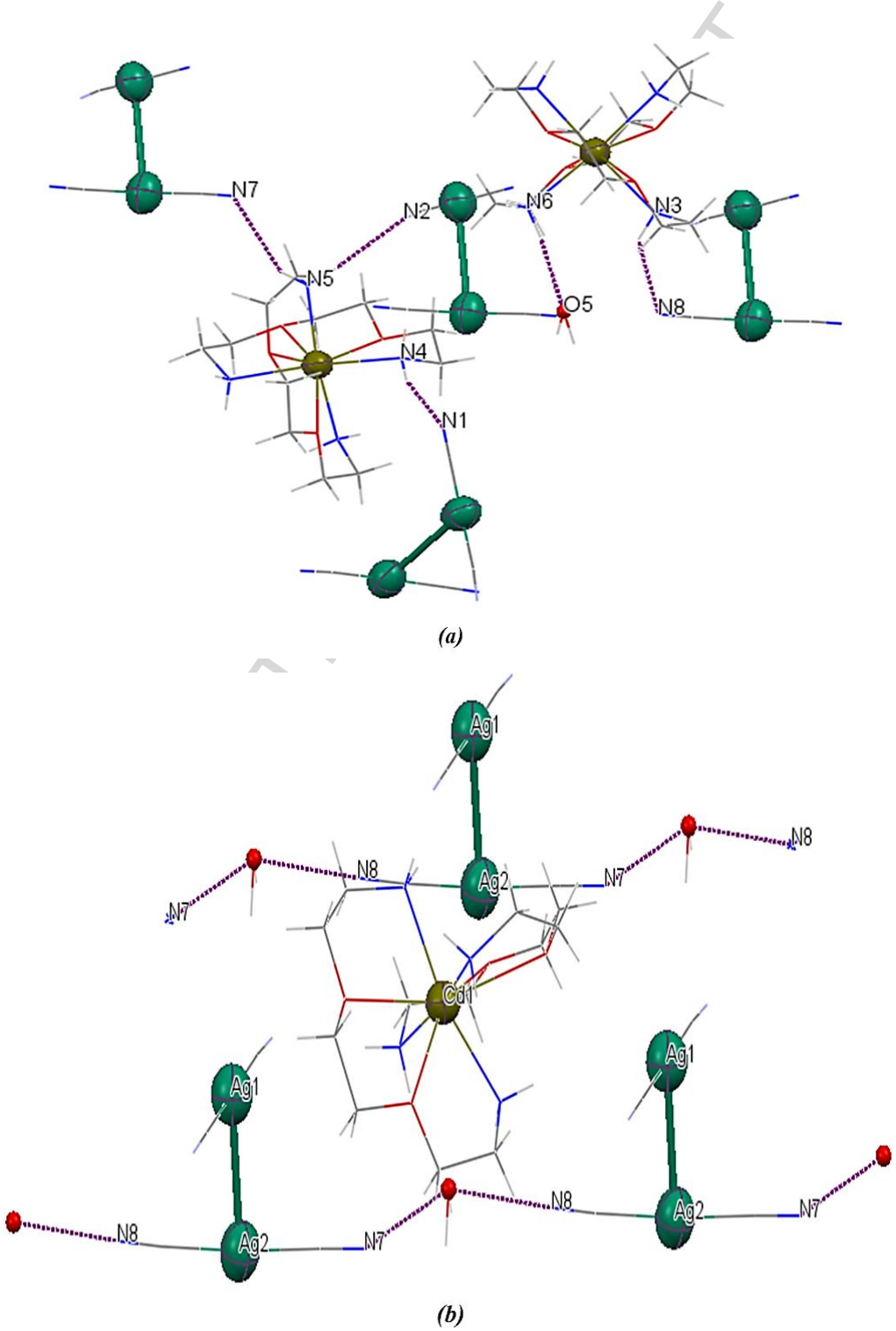

(a)

(b)

Figure 2. The hydrogen bonds between *edbea*-water, *edbea*-cyanido (***a***) and cyanido-water (***b***) in **4**

There are many hydrogen bonds mostly between *edbea* and cyanido ligands as seen in Figure 2a. There are also hydrogen bonds (Figures 2a and 2b) with water molecules, which act as both acceptor and donor in **4** (Table 2).

Table 2. Hydrogen bonds for **4** (Å and °)

D–H···A	*d(D–H)*	*d(H···A)*	*d(D···A)*	*<(DHA)*	*Symmetry codes**
N(3) -H(3C) ..N(8)*	0.90	2.54	3.236(14)	135	*-1+x, y, z*
N(4) -H(4D) ..N(1)	0.90	2.27	3.135(10)	162	-
N(5) -H(5C) ..N(7)*	0.90	2.49	3.240(12)	141	*-x, y-1/2, 1-z*
N(5) -H(5D) ..N(2)*	0.90	2.29	3.133(13)	157	*-x+1, -1/2+y, -z+1*
O(5)-H(5E) ..N(7)*	0.85	2.02	2.8682	172	*x, y, z+1*
O(5) -H(5F) ..N(8)*	0.86	1.95	2.8024	175	*-1+x, y, z*
N(6) -H(6D) ..O(5)	0.90	2.32	2.1828	160	-

2.2. EPR and Magnetic studies

For Ag^{I} and Ni^{II} ions, an EPR spectrum could not be observed, because Ag^{I} ion is diamagnetic and Ni^{II} ions may have short relaxation times at room temperature. The room temperature powder EPR spectrum of **2** is shown in Figure S4; Supplementary data. The values of $g_{//}$ and $g_{\perp}$ extracted from the powder spectrum were the following: $g_{//}$ = 2.164, $g_{\perp}$ = 2.060. These g parameters have indicated that the local symmetry of the paramagnetic center is axially symmetric. This spectrum belonged to Cu^{II} ion (S = 1/2, I = 3/2). From the order of $g_{//} > g_{\perp} > g_e$ (free electron *g* value, g_e = 2.0023), it could be concluded that Cu^{II} ions were located in tetragonal distorted octahedral sites (D_{4h}) elongated along the *z*-axis and the ground state of the paramagnetic electron was $d_{x^2-y^2}$ ($^2B_{1g}$ state) [38-41]. When the EPR spectra of the Cu^{II} complexes containing tetracyanidometallate and dicyanidoargentate were investigated, it was discovered that the spectroscopic splitting factors which is a measure of the rate of spin magnetic moments over spin angular momentum or Lande *g* values of these complexes were in the order of $g_{//} > g_{\perp} > g_e$ as it was in the complex **2** [14, 29, 42-47].

The magnetic susceptibilities of **1** and **2** were measured in the temperature range of 10–300 K. The temperature dependence of the molar magnetic susceptibility (χ_m) and $\chi_m T$ are shown in Figure S5 and S6 as Supplementary data for both complexes. As the temperature decreases, the value of the $\chi_m T$ increases continuously reaches a maximum around 20 K and then rapidly decreases on further cooling. The increase of $\chi_m T$ indicates the presence of intramolecular

ferromagnetic interaction. After 20 K, the drop of $\chi_m T$ value could be attributed to intermolecular antiferromagnetic couplings, as well as zero-field splitting for the Ni^{II} (**1**) or Cu^{II} (**2**). The magnetic data above 20 K for **1** was fitted by relation $C/(T-\theta)$ (Curie-Weiss Law), giving the best fit parameters as follows: $C = 1.354 \pm 0.0002\, emuK/mol.Oe$ and $\theta = 4.397 \pm 0.008\, K$. As for **2**, the temperature dependence of χ_m was fitted by the same formula. Determined fitting results were found as $0.175 \pm 0.0001 \frac{emuK}{mol}.Oe$ for C, $0.00054 \pm 0.000001\ emu/mol.Oe$ for α and $-0.16 \pm 0.006\, K$ for θ. Notice, the set of magnetic parameters for **1** and **2** showed a similarity to the tetracyanidometallate and dicyanidoargentate-based structures that we were previously reported [14, 29, 34, 42-47]. Also, cyanido-bridged heterometallic complexes generally exhibited antiferromagnetic interaction at low temperatures similar to the complexes **1** and **2** [42-46, 48,49].

The effective magnetic moments as Bohr Magneton of **1** and **2** were also calculated to be 3.29 μ_B and $1.18\,\mu_B$, respectively. It is said according to these results that **1** and **2** have a subnormal magnetic moment (3.87 μ_B for Ni^{II}, d^8 and 1.73 μ_B for Cu^{II}, d^9).

2.3. Biological properties

2.3.1. Antiproliferative effect of **2** *and* **3**

The anticancer activities of **2**, **3**, and $[Ag(CN)_2]^-$ to HeLa, HT29, C6, and Vero cell lines were evaluated using a BrdU cell elisa proliferation assay (Figure 3). The parent compound $[Ag(CN)_2]^-$ exhibited the most antiproliferative feature tested on all cells ($P < 0.05$), but it caused significant toxicity in all cells at concentrations of 1 μg/mL and higher (Figure 3). Therefore, $[Ag(CN)_2]^-$ can lead to necrosis more than apoptosis in cells, which may involve sudden corruption of cell membrane. **2** and **3** exhibited significantly ($P < 0.05$) strong antiproliferative activity than control compound towards the cancer cells tested, especially at 1.5 μg/mL and high concentrations.

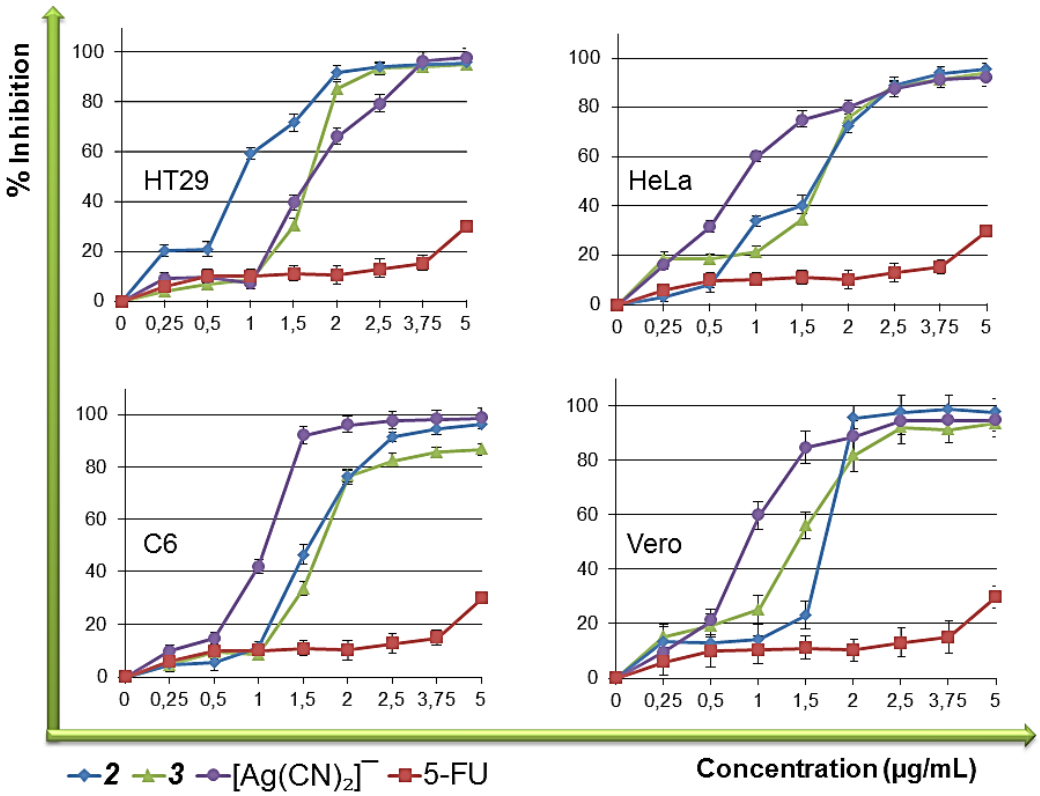

Figure 3. Effects of **2**, **3** and $[Ag(CN)_2]^-$ on the proliferation of HeLa, HT29, C6 and Vero cell lines. Percent inhibition noted is mean values ± SEM of three independent measures.

Table 3. IC50 values and tumor specificity rate for **2**, **3**, 5FU, and $[Ag(CN)_2]^-$

	IC50 (µM)				**Tumor specificity**		
Compounds	HeLa	HT29	C6	Vero	HeLa	HT29	C6
2	1.68	1.38	1.80	2.09	1.24	1.51	1.16
3	3.57	1.86	3.42	3.75	1.05	2.02	1.09
5FU	275.68	258.46	217.48	258.46	0.93	1.00	1.19
$[Ag(CN)_2]^-$	5.13	5.18	5.08	5.63	1.10	1.09	1.11

Moreover, **2** and **3** can lead to apoptosis more than necrosis in cells. We also found that the antiproliferative activities of **2** and **3** were lower on nontumorigenic Vero cells compared to cancer cells (Figure 3). IC50 values and tumor specificity rate to be used in subsequent studies were determined by performing ELISA BrdU assay, Table 3. Tumor-specificity was determined by the following equation:

Tumor-specificity for HT29 = IC50 (Vero)/IC50 (HT29); for HeLa = IC50 (Vero)/IC50 (HeLa); for C6 = IC50 (Vero)/IC50 (C6).

Both compounds showed good selectivity for the cancer cell line over the non-cancerous cell line. Therefore, the overall specificities of both compounds are ideal. The data of the cell proliferation inhibition displayed that the Ag^I complexes were significantly more effective than

conventional control anticancer drug (Figure 3), implying their antitumor potential, as in former studies [50-54].

2.3.2. Cytotoxic activity of **2** *and* **3**

The cytotoxic activities of **2**, **3**, $[Ag(CN)_2]^-$, and 5FU on HT29, HeLa, C6, and Vero cells were evaluated using an cytotoxicity measure kit based on lactate dehydrogenase. The cytotoxicity of **2** and **3** were much more lower than $[Ag(CN)_2]^-$ ligand, but they were close to the cytotoxicity of control anticancer drug at their IC_{50} and low concentrations (Figure 4). The percent cytotoxicity of **2**, **3**, and 5FU are calculated to be between 15 to 25 percent, whereas $[Ag(CN)_2]^-$ displayed nearly 60 percent cytotoxicity ($P < 0.05$) towards all cells (Figure 4).

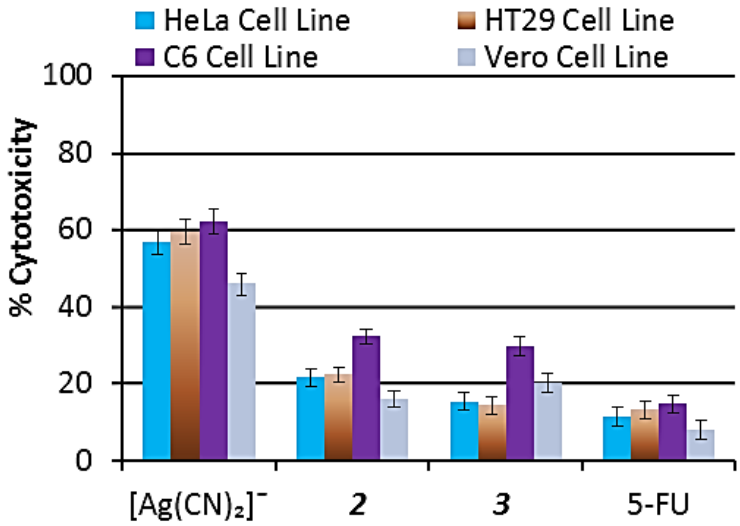

Figure 4. The cytotoxic activity of **2, 3** and $[Ag(CN)_2]^-$ on HeLa, HT29, C6 and Vero cell lines. Percent cytotoxicity was noted as mean values ± SDs of three independent measures

The LDH test results which are compatible to cell viability assay explained that both compounds may have cytostatic potential rather than cytotoxic affect especially at IC_{50} concentrations of **2** and **3.** The remarkable lower cytotoxicity of **2** and **3** may emphasize that the cytotoxicity of the parent molecule, $[Ag(CN)_2]^-$, reaches to safe levels by complexing with (2,2′-(ethylenedioxy)bis(ethylamine)) and (N,Nbis(2-hydroxyethyl)ethylenediamine) in **2** and **3**, without losing their antiproliferative features. Our results were similar to another study [55]. *In vitro* cytotoxicity studies also revealed that 1 and 4 are the most cytotoxic compounds against cell lines, and up to 9 fold higher than that of the control anticancer drug 5FU (data not shown).

*2.3.3. Detection of apoptotic potential of **2** and **3***

Here, to find whether the mechanism of anticancer and cytotoxicity of **2** and **3** resulted from apoptosis, we conducted *in vitro* DNA laddering property of **2** and **3** on HeLa, HT29 and C6 cells.

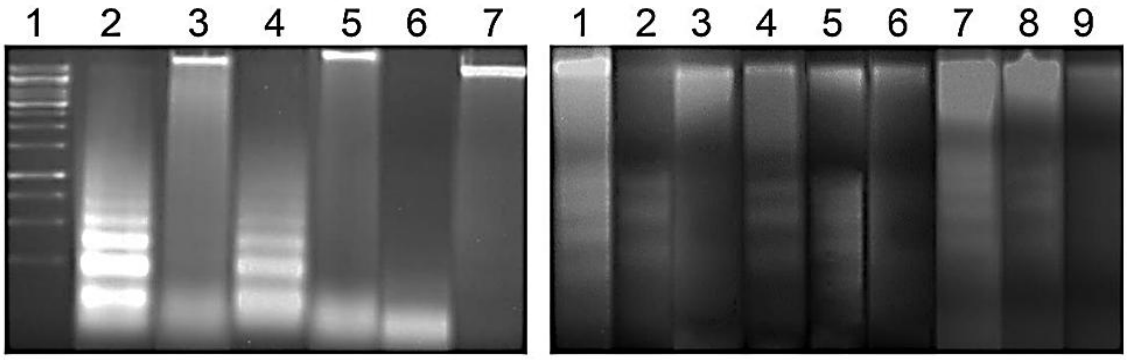

Figure 5. Effects of **2** and **3** on DNA fragmentation. Both **2** and **3** were caused DNA fragmentation. (A-**2**: Lane 1, DNA standard; Lane 2, HT29+**2**; Lane 3, HT29 Control; Lane 4, C6+**2**; Lane 5, C6 Control; Lane 6, HeLa+**2**; Lane 7, HeLa Control. B-**3**: Lane 1, C6+Camptothecin ; Lane 2, C6+**3**; Lane 3, C6 Control; Lane 4, HT29+Camptothecin ; Lane 5, HT29+**3**; Lane 6, HT29 Control; Lane 7, HeLa+Camptothecin; Lane 8, HeLa+**3**; Lane 9, HeLa Control)

There was no DNA laddering in untreated cells and genomic DNA remained intact in position near the top of the lanes. Here, appearances of apoptotic shapes and DNA laddering may be the result of a relationship between **2** or **3** and DNA. The DNA laddering test results explained both coordination complexes caused DNA fragmentation, an important marker of apoptosis (Figure 5). These results were consistent with antiproliferative and cytotoxic effect of **2** and **3**. These findings emphasized that **2** and **3** suppress the cell proliferation by triggering apoptotic mechanisms in favor of the results of previous studies [56, 57].

*2.3.4. Detection of apoptotic potential of **2** and **3** at a single cell level*

The apoptotic potential of **2** and **3** on HT29 cells was conducted using TUNEL test. As shown in Figure 6, **2**, **3**, and DNase I treated cells displayed shiny green fluorescence (TUNEL-positive) implying the fragmented DNA in apoptotic cell nucleolus, whereas the vehicle control was found to be TUNEL-negative. We have also examined phase-contrast images of the cells (***2′***, ***3′***, NC′ (negative control), and PC′ (positive control)) overlapping the fluorescence images of the cells (Figure 6). The TUNEL test exhibited an apoptosis in the HT29 cells in the presence of IC50 concentrations of **2** and **3** (1.01 μg/mL and 1.02 μg/mL, respectively) for 24 h. We evaluated image analysis of **2** and **3** in detail and both compounds

seriously caused more apoptosis in HT29 cells than the DNase I. In a previous study, a Ag^{I} complex, [Ni(*N-bishydeten*)$Ag_3(CN)_5$] acting as an apoptotic agent against HT29 cells, and exhibited TUNEL positive activity [51]. Nesrin and coworkers [34] showed that an antiproliferative good-soluble Ag(I) complexes, [Ni(*hydeten*)$_2$Ag(CN)$_2$] [Ag(CN)$_2$]·H_2O and [Cd_2(*hydeten*)$_2Ag_4(CN)_8$]·H_2O, similarly affected HT29 cells.

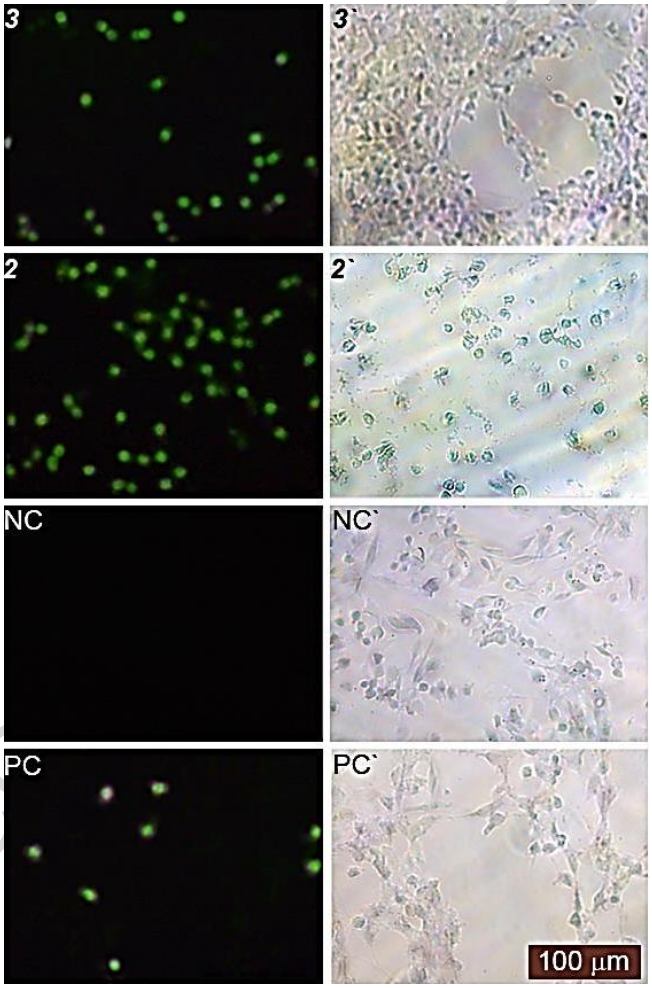

Figure 6.The picture represents fluorescence (**2**, **3**, NC, and PC) and phase-contrast (**2´**, **3´**, NC´, and PC´) images of the HT29 cells. NC: negative control, PC: positive control

2.3.5. Migration inhibitory behavior of **2** *and* **3**

The cell migration capability is a very significant cell feature and is an excellent source for druggability. The migration inhibitory feature of **2** and **3** was conducted using migration test on HeLa cells. Compounds **2** and **3** at IC_{50} concentrations exhibited a suppressive behavior on migrating HeLa cells in a time or dose dependent manner (Figure 7), suggesting they may have antimetastatic potential.

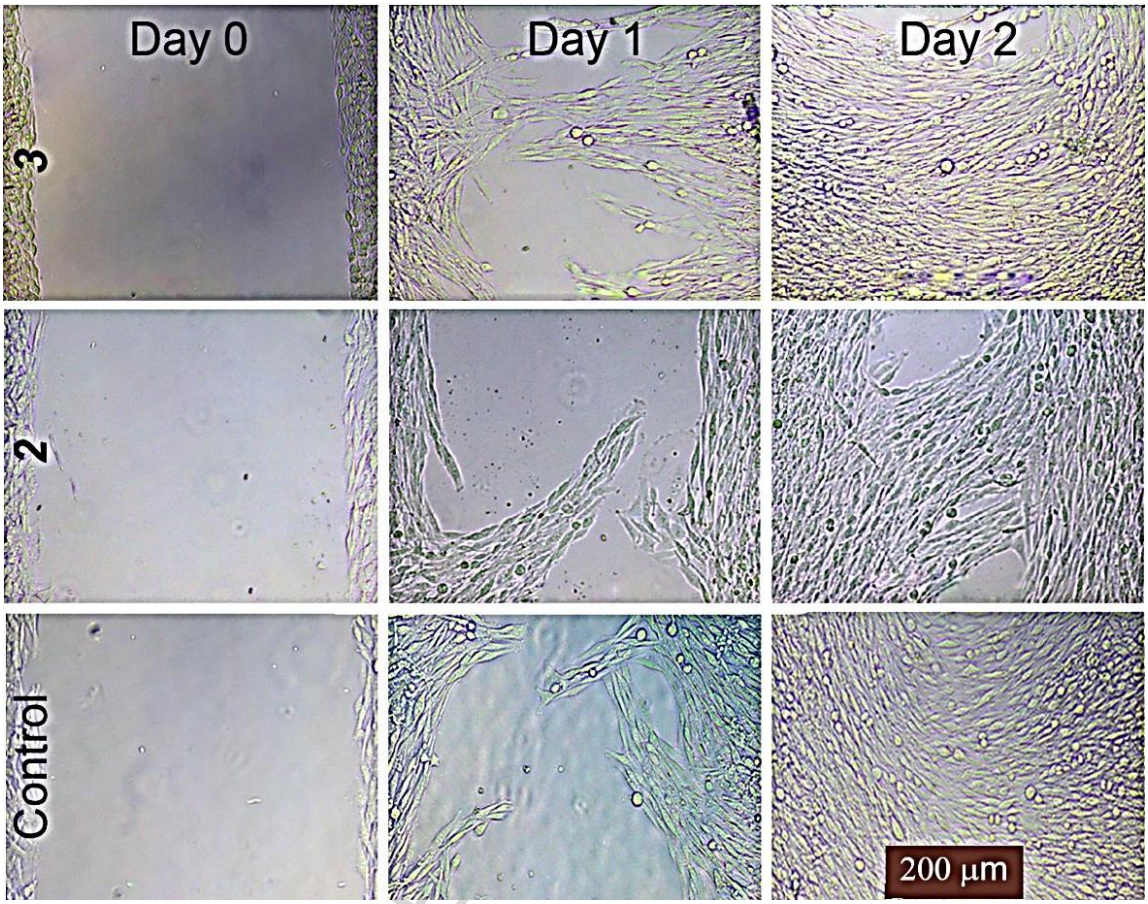

Figure 7.The image represents the effect of **2** and **3** on the migration of HeLa cells. The wound of the HeLa cells was photographed until the wound was filled by control cells. Note that the anti-migration effect of both on the cells became more apparent at day 2

Both compounds may also lead to progressed cell death due to apoptotic stress resulting from restricted cell migration. Arresting the cell migration is believed to affect the environmental and intracellular stress of the cancer cells according to the literature. The results obtained using a low concentration of **2** and **3** (< IC50) are quite similar to the literature [58-62]. Furthermore, **2** and **3** with low concentrations possess the ability to suppress cell migration without inhibiting cell division at non-toxic concentrations. After 72 h of incubation, the migration rate of the test compound-treated cells were significantly reduced (Figure 7, Day 2), and untreated HeLa cells accomplished to form a confluent monolayer, yet treated cells failed to form it. Our findings were consistent with some other studies have displayed that Ag^{I} complexes containing different ligands inhibit cell migration [63-64].

2.3.6. Detection of human topoisomerase I inhibitory effect of **2** *and* **3**

Human topoisomerase I is a nuclear enzyme and alter topological state of DNA through cut one of the two strands of double-stranded DNA resulting in facilitating vital cellular process,

including replication, transcription or DNA repair. Human topoisomerase I therefore is a significant druggability for chemotherapeutics. Several well-known topoisomerases inhibitors such as irinotecan, topotecan, and camptosar have been currently used in clinical routine for some cancer. Here, in order to find whether the antiproliferative activity of both compounds resulted from inhibition of human topoisomerase I, we evaluated the effects of our compounds on recombinant human topoisomerase I using relaxation assay of supercoiled plasmid DNA. As clearly shown in Figure 8, compound **2** or **3** considerably suppressed the DNA relaxation activity of human topoisomerase I, similar to the control anticancer drug, camptothecin. The findings suggest that **2** or **3** disrupts cell proliferation by the suppression of the human topoisomerase I activity during replication.

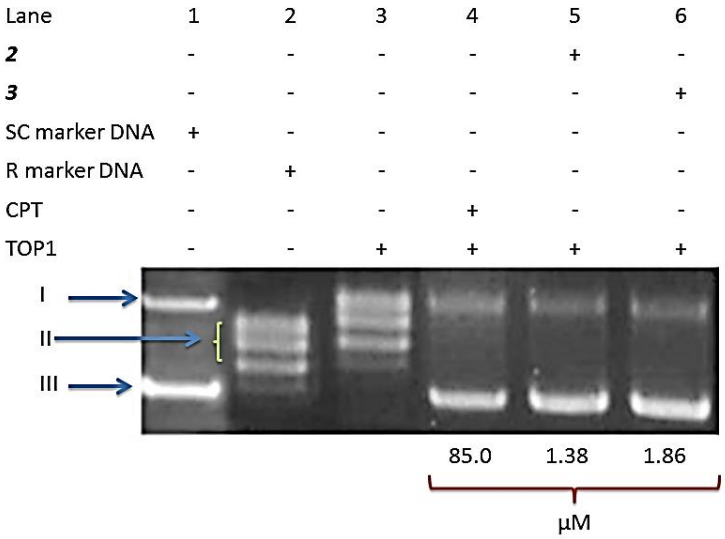

Figure 8.The image represents inhibition of recombinant DNA topoisomerase I activity by **2** and **3**. Lane 1: Supercoiled marker DNA; Lane 2: Relaxed marker DNA; Lane 3: Negative Control (Supercoiled DNA + Topo I); Lane 4: Positive Control (Supercoiled DNA + Topo I + Camptothecin); Lane 5: Supercoiled DNA + Topo I + **2**; Lane 6: Supercoiled DNA + Topo I + **3**

Similar to Wu's (2011) findings, these results show the binding of both complexes not only to human topoisomerase I, but also to other proteins or macromolecules such as human serum albumin, DNA and RNA [65]. It was noted by Hall et al. (1997) that Ni^{II} compounds of thiosemicarbazones significantly suppressed human DNA topoisomerase II [66]. Prabhakaran et al. (2011), similarly, displayed that Ni^{II} compounds consisting of N-substituted thiosemicarbazones remarkable inhibited human DNA topoisomerase II [67].

2.3.7. The effect of **2** *and* **3** *on the morphology of cells*

The effects of the 2 and 3 on the morphology of the cells were photographed (Figure 9). Both compounds clearly blocked the development and growth of the cells and decreased the quality and the number of the cells in the flask surface. The cells exhibited very weakly clinched the surface of the cell plate and become globular upon application. HT29 and C6 cells deformed their fibroblast like appearance clumping together of cells. Apoptotic sample cells demonstrated cytoplasmic blebs or shrinkages, and persistent declining in cell volume as specific apoptotic markers. These findings resemble to previous studies by Aydın et al., Karadağ et al., and Tekin et al. [50-54]. Overall, according to our current knowledge of literature, the appearance of the subjected to cells obviously showed the antiproliferative and sustainable cytotoxic effect of both compounds.

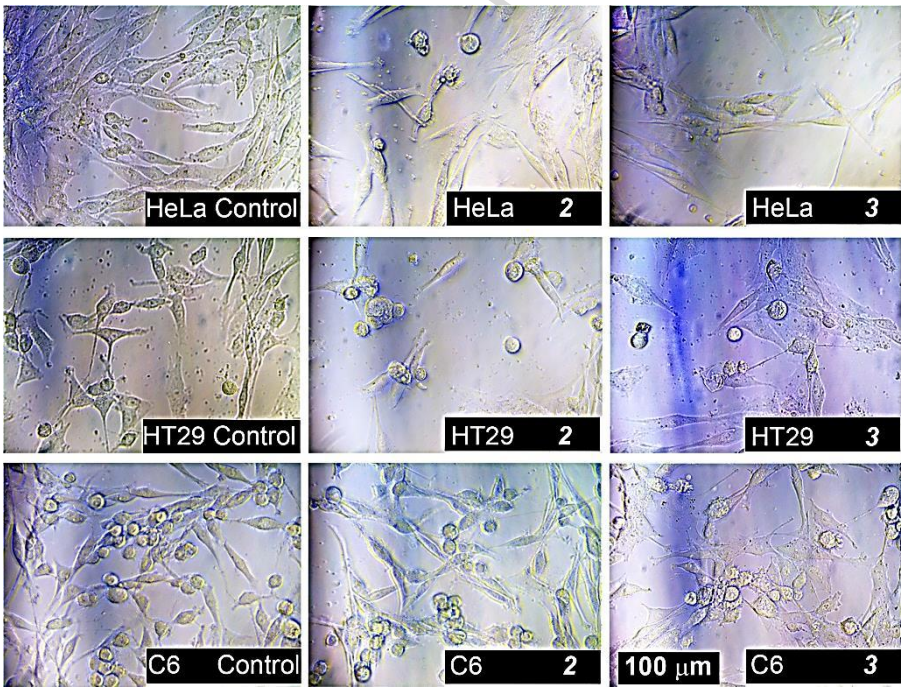

Figure 9. The image represents the effect of **2** and **3** on the morphology of the cells. DMSO treated cells as vehicle

2.3.8. IHC study

Immunohistochemistry staining of sectioned slides showed decreased expression of Bcl-2 and increased accumulation of P53 as an expected observation in point of cell survival in Ag^{I} complexes-treated cells, which indicates the apoptotic action of both compounds (Figure 10). There are closed aspects of these findings with relevant literature [68]. The results also showed that Ag^{I} complexes execution into cells caused significantly decreased the expression of CK20 (a marker protein for HT29 cells) and CK7 (a marker protein for HeLa cells). Cytokeratins

releasing from proliferating or apoptotic cells may change cell characteristics through altering mRNA levels. Decrease CK7 and CK20 can be associated with the inhibited metastatic ability influencing intermediate filament (IF) proteins (Figure 10).

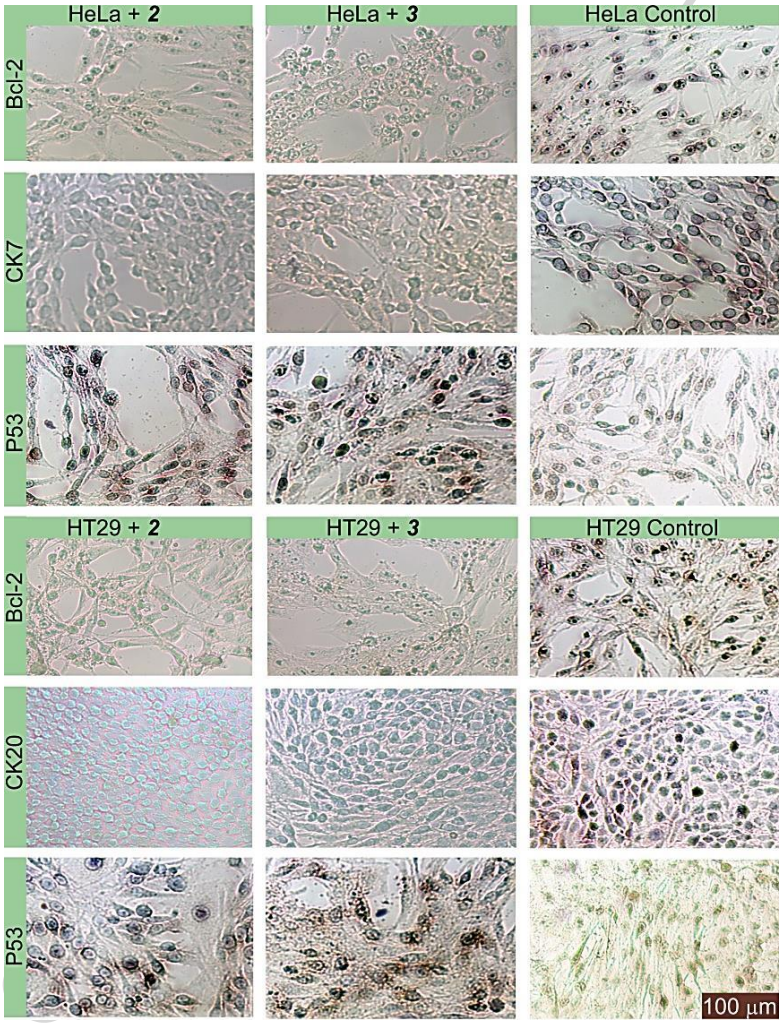

Figure 10. Representative images of the cells examined by immunohistochemical staining for functional protein group (Bcl-2 and P53), and for marker protein group (CK7 and CK20). The specific signals are shown as brown staining

2.3.9. Antibacterial Activity

The antimicrobial activities of **1-4** were tested *against* one yeast (*Candida utilis* KUEN 1031), four gram-positivebacteria (*Staphylococcusaureus* ATCC 29213, *Bacillus subtilis* ATCC 6633, *Bacillus cereus*DSM 4312, *Streptococcus pyogenes* ATCC 176), and five gram-negative bacteria (*Escherichia coli* 111, *Escherichia aerogenes* 2924, *Salmonella gallinarum*, *Pseudomonas aeruginosa* ATCC 27859, and *Salmonella enteridis* ATCC 13076) using the disc-diffusion method. The SCF [Sulbactam (30 µg) + Cefoperazone (75 µg)] and KCN were used as standard drugs. The experiments were conducted in triplicate to minimize possible

errors. The inhibition zone caused by each compound was measured. The results of antibacterial studies were presented in Table 4. The screening results demonstrated that the compounds **1**, **2**, **3**, and **4** have a considerably antimicrobial activity. In effect, **3** was more effective than the positive control (SCF) for all of the bacteria.

Usually, all bacteria from the data in Table 4 exhibited a sequence **3** > **4** > SCF > **2** > **1** > KCN for antibacterial activity. For *S. enteridis* and *S. gallinarum*, the data in Table 4 exhibited **3** >**4** > SCF > **2** > **1** > KCN sequence of antibacterial effect. The values of 45 and 41 mm made it obvious that the antibacterial effect of **3** was the strongest among all.

Table 4. Antibacterial activity of ***1-4*** (105 µg/disc)

Microorganisms	Compounds and inhibition zones (mm)					
	SCF	**KCN**	**1**	**2**	**3**	**4**
Gram-positive bacteria						
S. aureus ATCC29213	29	-	16	26	33	32
B. subtilis ATCC6633	19	-	23	25	35	30
B. cereus DSM 4312	30	-	29	30	35	28
St. pyogenez ATCC176	20	-	24	30	40	30
Gram-negative bacteria						
E. coli 111	21	-	19	35	39	29
E. aerogenes 2924	31	-	26	30	35	27
S. gallinarum	30	-	19	25	41	35
P. aeruginosa ATCC9027	15	-	30	31	35	27
S. enteridis ATCC13076	22	-	30	31	45	35
Yeast						
C. utilis KUEN1031	19	-	21	33	34	30

SCF, sulbactam (30 µg) + cefoperazone (75 µg), as a positive control
KCN, potassium cyanide, as a negative control

Based on the preliminary screening data, compounds **1**, **2**, **3** and **4** were subjected to MIC (minimum inhibitory concentrations) studies. The findings are submitted in Table 5. Sulbactam (30 µg) + Cefoperazone (75 µg) (105 µg/disc) used as a positive control were evaluated using Serial microdilution method that was performed to determine MIC values in Mueller–Hinton Broth for antibacterial test. The measurable inhibition zones and MIC values for *C. utilis* isolates for **1-4** were found in the range of 21-34 mm and 125-250 µg/mL, respectively. The measurable inhibition zones and MIC values for bacterial strains for **1-4** were found in the range of 16-45 mm and 15.62-250 µg/mL, respectively (Tables 4 and 5). Four gram positive bacterial strains (*S. aureus, B. subtilis, B. cereus* and *St. pyogenez*) and five gram negative (*E. coli, E. aerogenes, S. gallinarum, P. aeruginosa* and *S. enteridis*) were sensitive to **1-4**. In the case of **3**, the measurable inhibition zones and MIC values of the bacterial strains were found 33-45 mm and 15.62-62.5 µg/mL, respectively (Tables 4 and 5).

These data revealed that the **3** has the strongest antibacterial effect due to higher inhibition zone than the standard drug SCF and other complexes (**1**, **2** and **4**).

Table 5. Minimum-inhibitory concentrations (MIC, in mg/mL) of **1-4**

Microorganisms	Antibiotics MIC (µg /mL)					
	KCN	**1**	**2**	**3**	**4**	**SCF**
Gram-positive bacteria						
S. aureus ATCC29213	-	125	62.50	15.62	31.25	250
B. subtilis ATCC6633	-	250	31.25	15.62	31.25	500
B. cereus DSM 4312	-	31.25	125	31.25	62.50	500
St. pyogenez ATCC176	-	125	62.50	15.62	62.25	500
Gram-negative bacteria						
E. coli 111	-	250	31.25	15.62	31.25	250
P. aeruginosa ATCC9027	-	62.50	62.50	31.25	62.25	1000
E. aerogenes ATCC2924	-	125	31.25	31.25	125	62.50
S. gallinarum	-	125	62.50	15.62	62.25	62.50
S. enteridis ATCC13076	-	62.50	15.62	31.25	125	1000
Yeast						
C. utilis KUEN1031	-	125	250	62.5	125	500

SCF, sulbactam (30 µg) + cefoperazone (75 µg), as a positive control
KCN, potassium cyanide, as a negative control

As seen in the Table 5, complex **3** (MIC: 15.62, 15.62, 15.62, 15.62, 31.25, 31.25, 15.62, 31.25, 62.5 µg/mL, respectively) exhibited better activity than other complex (**1**, **2**, **4**) and the positive control for *S. aureus, B. subtilis, St. pyogenez, E. coli, P. aeruginosa, E. aerogenes, S. gallinarum, S. enteridis* and *C. utilis* bacteria.

2.3.10. Antifungal activity

In the mycelial growth of the pathogens *Alternaria solani*, *Rhizoctonia solani*, *Fusarium oxysporum*, and *Sclerotinia sclerotiorum*, the Ag^{I} compounds (**1**- **4**) exhibited various levels of efficiency of inhibition over control (50 % DMSO) at different concentrations. However, **2** was non-effective against the fungi tested at any of the concentrations. All the findings obtained from five different concentrations were considered in terms of their mean value (Table 6 and 7). Compound 3 exhibited the maximum mycelial growth inhibition on *A. solani* with 97.3 % at 20 µg/mL concentration (Table7) and followed by **4** and **1** with 96.8 % and 92.8 % inhibitions respectively. At 20 µg/mL, maximum mycelial growth inhibition was observed on *R. solani* with compound **3** (Table 7) andfollowed in the same order of the other compounds above. Compounds **1**, **3**, and **4** inhibited mycelial growth of *S. sclerotiorum* with 90 % or higher levels at 15 to 20 µg/mL concentrations (Table 8). Each compound had higher inhibitory effect against *A. solani* excluding **1** with low inhibitor effect towards *R. solani* and *F. oxysporum* (Table 7 and 8). Even at the highest concentration, compound **2** did not inhibit

the mycelia growth of all the tested fungi (Table 6 and 7). At 5 µg/mL or higher concentration inhibitory effects of test compounds against *S. sclerotiorum* were found to be statistically significant compared to DMSO and fungicides (Maneb and Copper hydroxide).

Table 6. Antifungal activities of Ag^{I} compounds against two plant pathogenic fungi after 5 days

Dosage(µg/mL)/ Chemicals	*Alternaria solani* (Growth inhibition %)				*Rhizoctonia solani* (Growth inhibition %)			
	1	**2**	**3**	**4**	**1**	**2**	**3**	**4**
20.0	92.8^{a}	0.0	97.3^{a}	96.8^{a}	58.4^{a}	0.0	78.3^{a}	82.2^{a}
15.0	85.2^{b}	0.0	94.6^{a}	95.1^{a}	54.5^{a}	0.0	73.9^{b}	71.5^{b}
10.0	71.7^{c}	0.0	83.8^{b}	88.8^{b}	48.2^{b}	0.0	65.4^{c}	68.8^{b}
7.5	62.1^{d}	0.0	81.8^{bc}	61.2^{d}	49.5^{b}	0.0	51.5^{d}	48.6^{c}
5.0	56.6^{e}	0.0	79.0^{c}	54.7^{e}	39.6^{c}	0.0	28.2^{e}	42.2^{d}
Maneb Cupper Hydroxide	67.8^{c}		67.8^{d}	67.8^{c}	20.0^{d}		20.0^{f}	20.0^{e}
DMSO (50%)	0.0^{f}	0.0	0.0^{e}	0.0^{e}	0.0^{e}	0.0	0.0^{g}	0.0^{f}
LSD	4.0		3.7	4.9	3.9		2.8	2.9

***** Means in a column followed by the same letter are not significantly different (ANOVA, P < 0.05)

Table 7. Antifungal activities of Ag^{I} compounds against two plant pathogenic fungi after 5 day

Dosage(µg/mL)/ Chemicals	*Fusarium oxysporum* (Growth inhibition %)				*Sclerotinia sclerotiorum* (Growth inhibition %)			
	1	**2**	**3**	**4**	**1**	**2**	**3**	**4**
20.0	68.0^{b}	0.0	75.4^{ab}	89.3^{a}	100.0^{a}	0.0	97.3^{a}	99.5^{a}
15.0	67.2^{b}	0.0	74.9^{b}	77.4^{b}	100.0^{a}	0.0	94.7^{a}	97.7^{ab}
10.0	63.4^{c}	0.0	73.6^{b}	69.4^{c}	98.3^{b}	0.0	74.7^{b}	96.8^{b}
7.5	59.7^{d}	0.0	68.3^{c}	67.7^{cd}	96.5^{c}	0.0	60.8^{c}	93.3^{c}
5.0	50.7^{e}	0.0	66.8^{c}	62.4^{d}	93.3^{d}	0.0	0.0^{d}	92.2^{c}
Maneb Cupper Hydroxide	78.0^{a}		78.0^{a}	78.0^{b}	0.0^{e}		0.0^{d}	0.0^{d}
DMSO (50%)	0.0^{f}	0.0	0.0^{d}	0.0^{e}	0.0^{e}	0.0	0.0^{d}	0.0^{d}
LSD	3.3		2.6	6.3	0.3		3.2	1.9

* Means in a column followed by the same letter are not significantly different (ANOVA, P < 0.05)

Table 8. Probit analysis parameters from the dose-response test performed with the **1, 3,** and **4**

Compound	Bioassay	Slope (±SE)[a]	LC50 (95% of fiducial limits	LC90 (95% of fiducial limits)	$\chi 2^{b}$
1	*A. solani*	2.25±0.331	5.46 (4.18-6.47)	20.2 (16.33-28.77)	2.1
	F. oxysporum	0.85±0.295	3.96 (0.52-6.27)	125.24 (43.72-2629.0)	1.12
3	*A. solani*	1.46±0.355	2.24 (0.60-3.66)	16.83 (12.77-31.59)	2.68
	S. sclerotiorum	5.28±0.426	8.29 (7.26-9.30)	14.5 (12.55-18.9)	35.26
4	*A. solani*	3.21±0.396	5.19 (4.29-5.92)	12.10 (11.41-15.66)	11.7
	R. solani	2.12±0.316	6.31 (4.98-7.39)	25.37 (19.69-39.24)	3.41
	F. oxysporum	1.38±0.326	3.07 (1.10-4.60)	26.21 (18.05-66.69)	6.53
	S. sclerotiorum	1.79±0.632	0.82 (0.005-2.12)	4.26 (1.0-6.03)	5.08

[a]Slope of the concentration (± standard error) response of the fungi to ***1, 3,*** and ***4***
[b]Pearson chi-square goodness-of-fit test on the probit model (α=0.05)

The calculated LC50 and LC90 values of **1**, **3**, and **4** using probit analysis to mycelial growth of four plant pathogenic fungi are exhibited in Table 8. The LC 50 and LC90 values of the three compounds ranged from 0.82 µg/mL to 8.29 µg/mL and 4.26 µg/mL to 125.24 µg/mL, respectively. The LC50 and LC90 values of compound **4** against *S. sclerotiorum* were 0.82 µg/mL and 4.26 µg/mL, respectively andfollowed by *A. solani* (Table 8). These findings implied that **4** can be used against either pathogenic fungus as a fungicide. Similarly, the other effective compounds (**1** and **3**) are promising fungicide candidates against *A. solani*. This is the first report of the inhibitory effects of the compounds against above mentioned fungi.

2.3.11. DNA/BSA binding and gel electrophoresis studies

Complex–DNA affinity can be conducted by observing UV–Vis absorption spectral data of free complex and complex–DNA adducts. The binding constant (K) of the **2** or **3** with DNA can be calculated with the help of Benesi–Hildebrand equation, $A_0/A\text{-}A_0=\varepsilon_G/\varepsilon_{H-G}\text{-}\varepsilon_G+\varepsilon_G/\varepsilon_{H-G}\text{-}\varepsilon_G x 1/K[DNA]$, where K is the binding constant, A_0 and A are the absorbances of the **2** or **3** and its adduct with DNA, respectively, and ε_G and ε_{H-G} are the absorption coefficients of the complexes and the complex–DNA adduct, respectively. The binding constant can be calculated using the intercept-to-slope ratios of $A_0/(A - A_0)$ vs. 1/[DNA] plots. Figure 11*A*, describes the interaction of Ag^I complexes with CT-DNA. According to Benesi–Hildebrand equation, the plot of $A_0/(A–A_0)$ vs. 1/[DNA] data yielded the binding constant (K) which was 1.3×10^4 M^{-1} for **2**, and 9.9×10^3 M^{-1} for **3** (Figure 11*A*). With the increase in CT-DNA concentration resulted in hyperchromic effect indicate a strong interaction between these complexes and DNA. This hyperchromic effect on the spectra of the complex-DNA adduct might be indicative of groove binding. Isosbestic points near 260 – 261 nm and 265 - 266 nm was observed for the **2** (Figure 11*A*).

The interaction of these complexes with BSA can be evaluated by observing of the UV–Vis absorption and emission spectral data of the free complex and complex–BSA adduct. The absorption spectral data of the compounds (25 µM) in altering concentrations of the BSA (0 - 100 µM) is shown in Figure 11*B*. **3** caused an increase in the absorbance of BSA and exhibited a slight blue shift, indicating a Van der Waals interactions or hydrogen bonds in affinity with BSA. Isosbestic points near 265 - 266 nm was observed for the **2** (Figure 11*B*).

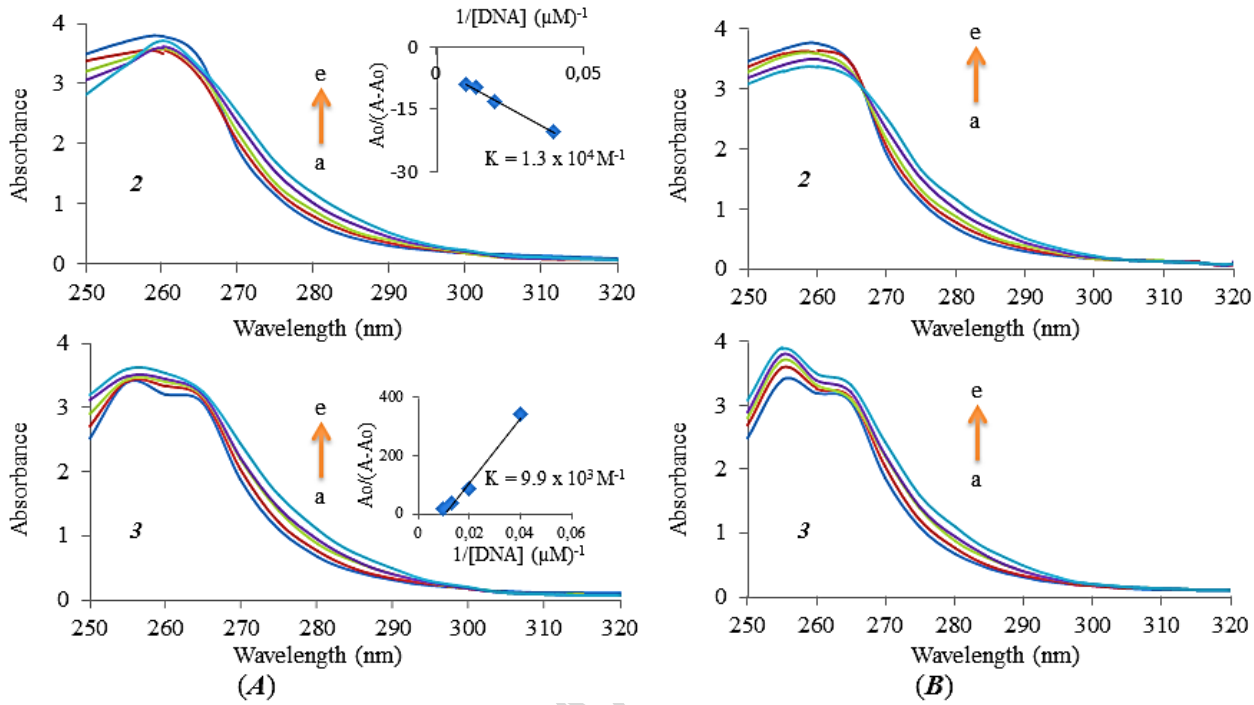

Figure 11. (***A***) UV–Visible absorption spectra of 25 μM **2** and **3** in the absence (a) and presence of 25 μM (b), 50 μM (c), 75 μM (d) and 100 μM (e) DNA. Note: The direction of arrow represents rising concentrations of DNA. Inside graph is the plot of $A_0/(A–A_0)$ vs. 1/[DNA] to find the binding constant of the complex–DNA adduct. (***B***) Absorption spectra of 25 μM **2** and **3** (a) in presence of different concentrations of BSA 25 μM (b), 50 μM (c), 75 μM (d), and 100 μM (e). Note: The direction of arrow represents rising concentrations of BSA

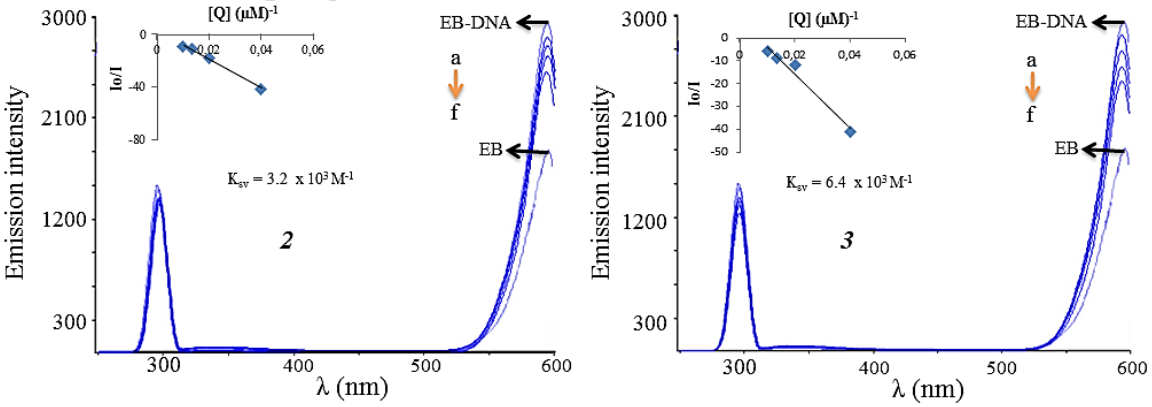

Figure 12. The emission spectral data of EB-bound (a) DNA solutions in the absence and presence of increasing concentrations of these complexes 25 μM (b), 50 μM (c), 75 μM (d), and 100 μM (f). [EB]=10.0 μM (a), [DNA] 50.0 μM. The arrows show the changes in severity upon increasing amounts of **2** or **3**. Inset shows the plots of emission severity I_0/I vs. [Q] (μM) for determining K_{SV}

The emission spectral data of EB bound to DNA in altering concentrations of the complexes are available in Figure 12. According this data, **2** or **3** intercalating into DNA resulted in decreasing the fluorescence severity of the EB-DNA adduct and the level of this reduction displayed binding constant of both. The extent of quenching severity of EB bound to CT-DNA by **2** or **3** is shown in Figure 12. The quenching of EB bound to CT-DNA by these complexes is displayed the linear Stern–Volmer equation ($I_0/I = 1 + K_{SV}$ [Q]), which provides data of **1** or **2** binding mechanism information. The K_{SV} value for **2** and **3** are 3.2 x 10^3 M^{-1}, and 6.4 x 10^3 M^{-1}, respectively suggesting the affinity of **3** with CT-DNA is robuster than that of **2**.

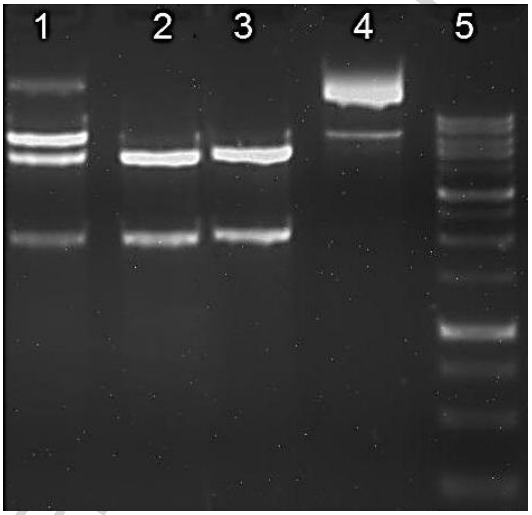

Figure 13. Inhibition of KpnI and BamHI restriction endonucleases activity. Following 4 h 37°C digestion of the 14µL with 10 U KpnI and BamHI, these digestion products were resolved with 1.5% agarose gel containing ethidium bromide. Lane 1: enzyme + DNA + **3**, Lane 2: enzyme + DNA + ***2***, Lane 3: Positive control (enzyme + DNA), Lane 4: Negative control (plasmid DNA + water); lane 5: DNA marker (1Kb)

After KpnI and BamHI digestion of pTOLT plasmid DNA, digestion products were identified by two DNA bands in the absence complexes (Lane 3), whereas in the presence of the **3** produced four bands (Lane 1), and the **2** displayed two bands DNA fragments (Lane 2) (Figure 13). In the presence of **3** DNA digestion was incomplete and new bands were observed near the well at the top of the lanes (Lanes 1). Treatment of KpnI and BamHI with **3** inhibits the restriction endonucleases activity of these enzymes and new band attributed to the whole plasmid. The results indicated that **3** probably bound to pTOLT plasmid DNA. However, **2** failed to inhibit these enzymes, and resulted in the formation of two bands (Lane 2) (Figure 13).

2.4. Stability Study

Simple spectrophotometric methods were used for the stability features of these compounds in physiological buffer. For the stability studies with these compounds, a 5 mM stock solution of each of the silver compounds was prepared in 8.00 mL Tris–HCl buffer. The working solution was prepared by adding 0.1M phosphate buffer to obtain a volume range from 5 to 100 µg/mL. The compounds in physiological buffer were analyzed over the 3-day study period at least 3 times. The silver compounds exhibited strong stability in phosphate buffer (Table 9). Intraday measurement displayed that these compounds remained fairly stable. The linearity, precision and accuracy of the compounds are within acceptable limits for UV-Vis spectrophotometric method (Figure 14*A*, Table 9). The spectrum of the compounds demonstrates a slight increase in the peak from the second and third day to the finish of the study (Figure 14*B*, Table 9). These results displayed that the compounds in solution were found stable up to 72 h at room temperature.

Table 9. Results of UV-Vis spectrophotometric method

Parameters / Compounds		**1**	**2**	**3**	**4**
Linearity		0,9546	0,9962	0,9804	0,9883
Accuracy, % RSD < 2%		19,34	10,19	7,16	7,89
Precision, % RSD < 2%	Repeatability	3,24	4,61	8,13	1,63
	Intraday	2,74	6,00	8,14	1,64
	Interday	8,40	23,21	4,99	2,39
LOD		25,50	7,21	16,53	12,68
LOQ		77,27	21,87	50,09	38,45
% Error		8,65	4,55	3,20	3,52
Linearity range		5-100	5-100	5-100	5-100

Eight points calibration curve were obtained in a concentration range from 5-100 µg/mL for these compounds. The plots in measuring of the compounds was found to be linear in the scanning concentration range and the linearity values of **1**, **2**, **3**, and **4** were 0.9546, 0.9962, 0.9804, and 0.9883 (Table 9). The UV-Vis spectrophotometric method results demonstrated that the %RSD values of **1**, **2**, **3**, and **4** for the repeatability for precision studies were within acceptable limits and were 3.24, 4.61, 8.13, and 1.63, respectively (Table 9). The LOQ values of **1**, **2**, **3**, and **4** were 77.27, 21.87, 50.09, and 38.45 µg/mL, respectively. Based on these results, these compounds stability features were enough to meet specific acceptance criteria of ICH Q2(R1) guideline.

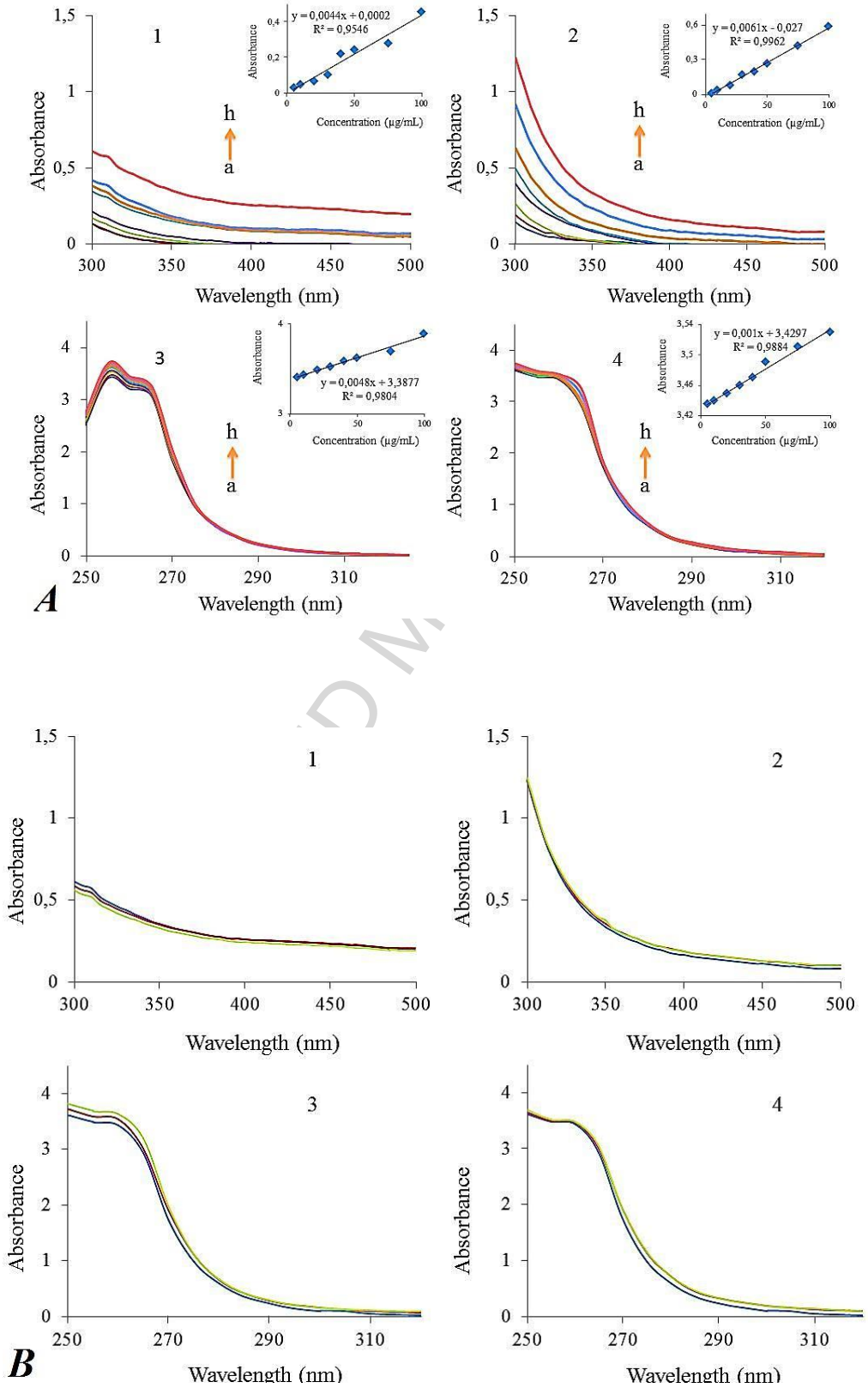

Figure 14. (***A***) The spectrum data of the compounds in following concentrations: 5 (a), 10 (b), 20 (c), 30 (d), 40 (e), 50 (f), 75 (g), and 100 µg/mL (h). Note: Inside graph is the linearity curve for these compounds. (***B***) The stability of the compounds (100 µg/mL) in 0.1M phosphate buffer (pH 7.4) at 37°C. Spectra collected once every day for 3 day.

3. Conclusions

As a result, Ni^{II} Cu^{II} and Cd^{II} centered bimetallic argentate complexes were synthesized by mixing metal salts and *edbea* with $K[Ag(CN)_2]$ and were characterized by various spectroscopic and analysis methods. According to *X*-ray spectra, the complex **4** consists of an ionic structure which is of $[Cd(edbea)_2][Ag(CN)_2]_2.H_2O$ general formula. The *EPR* analysis showed that all of the Cu^{II} underwent tetragonal distortion and the ground state of the paramagnetic electron was $d_{x^2-y^2}$ ($^2B_{1g}$ state). Magnetic susceptibility measurements of the complexes revealed that $[Ni(edbea)Ag_3(CN)_5]$ (**1**) was reached a maximum of intramolecular ferromagnetic interaction at 20 K and exhibited intermolecular antiferromagnetic interaction above 20 K, while $[Cu(edbea)Ag_2(CN)_4].H_2O$ (**2**) showed weak antiferromagnetic interactions below about 10 K. The binding of **2** or **3** to CT-DNA and BSA resulted in significant changes in spectral characteristics. The complexes showed hyperchromic absorption spectra and interacted directly with CT-DNA in a manner to groove binder. The complexes were the result of the tendency of a Van der Waals forces or hydrogen bonds during affinity with BSA. The fluorescence emission of **2** and **3** was efficiently quenched, which indicated that the compounds are directly located to CT-DNA groove. According to our findings the compounds demonstrated very potent antimicrobial (**1-4**), antifungal (**1-4**) and anticancer activities (**2** and **3**). We have explained for the first time that our compounds are robust apoptosis inducers, topoisomerase I inhibitors and migration suppressors. We also showed that treatment of cells with these compounds resulted in loss of Bcl-2 and accumulation of P53. The essence of the study is that these compounds are potentially significant drug candidates and are suitable to enter to the phase studies.

4. Experimental

4.1. Preparations of complexes

$AgNO_3$, KCN, $NiCl_2.6H_2O$, $CuCl_2.2H_2O$, $CdSO_4.8/3H_2O$, $Cd(CH_3COO)_2.2H_2O$ and 2,2′-(ethylenedioxy)bis(ethylamine) (*edbea*) were used as received. The syntheses of **1**–**4** carried out at room temperature are made according to the following general procedure: The solution of $AgNO_3$ (200 mg, 1.177 mmol) in water/alcohol was added to a magnetically stirred 153 mg or 1.175 mmol KCN. Then, the second metal salt (1 mmol) was added to resulting solution in a couple of minutes. Afterwards, the resulting slurry was added to the alcohol solution of 350 mg or 1.180 mmol *edbea* dropwise with vigorous stirring and the newly formed solution (except for **1**) was stirred approximately for 2-3 hours. Finally, the resulting product was filtered, washed in alcohol and water, and dried at room conditions. Pink precipitate was

obtained with 70 % yield for complex **1**. Anal. Calc. for $C_{11}H_{16}N_7O_2Ag_3Ni$: C, 20.00; H, 2.44; N, 14.84. Found: C, 19.75; H, 2.56; N, 14.45 %. IR (KBr disk; cm^{-1}) 3342, 3276 [υ(N–H)]; 2944, 2906, 2865 [υ(C–H)]; 2161 [υ(C≡N)]. Dark blue precipitate was obtained with 35 % yield for complex **2**. Anal. Calc. for $C_{10}H_{18}N_6O_3Ag_2Cu$: C, 21.85; H, 3.30; N, 15.29. Found: C, 21.93; H, 3.57; N, 15.66 %. IR (KBr disk; cm^{-1}) 3434 [υ(O–H)]; 3282, 3162 [υ(N–H)]; 2925, 2873 [υ(C–H)]; 2163, 2138 [υ(C≡N)]. Colorless precipitate was obtained with 54 % yield for complex **3**. Anal. Calc. for $C_{11}H_{18}N_7O_3Ag_3Cd$: C, 18.04; H, 2.48; N, 13.39. Found: C, 18.89; H, 2.41; N, 13.69 %. IR (KBr disk; cm^{-1}) 3631 [υ(O–H)]; 3322, 3291, 3256 [υ(N–H)]; 2919, 2875 [υ(C–H)]; 2157, 2140 [υ(C≡N)]. Colorless crystals suitable for single-crystal X-ray diffraction were obtained with 62 % yield for complex **4**. Anal. Calc. for $C_{16}H_{34}N_8O_5Ag_2Cd$: C, 25.74; H, 4.59; N, 15.01. Found: C, 26.53; H, 5.66; N, 16.08 %. IR (KBr disk; cm^{-1}) 3631 [υ(O–H)]; 3378, 3336, 3282 [υ(N–H)]; 2923, 2897, 2897 [υ(C–H)]; 2154 [υ(C≡N)].

4.2. Physical Measurements

C, H and N analyses were carried out with a LECO CHNS-932 elemental analyzer. FT-IR spectra were recorded with a Jasco 430 FT-IR spectrometer as dry KBr pellets from 400 to 4000 cm^{-1}. Thermal gravimetric analyses (TGA) were performed on a Perkin-Elmer Diamond TG/DTA thermoanalyzer under nitrogen (35–1200 °C range) at a heating rate of 10 °C min^{-1}. The magnetization measurements were carried out on a Quantum Design PPMS system at 10–300 K. χ–T graphs were recorded under the constant magnetic field of 0.5 kOe. Magnetic data were corrected for the diamagnetic contribution of the sample holder.

4.3. X-ray Structure Determination

The crystallographic data collections for **4** were carried out on a Rigaku R-AXIS RAPID-S imaging plate diffractometer using graphite-monochromated MoKα radiation (λ=0. 71073 Å) and oscillation scan technique with $\Delta\omega$=5˚ for one image were used for data collection. Integration of the intensities, correction for Lorentz and polarization effects and cell refinement was performed using CrystalClear software [69]. The structure was solved by direct methods and refined against F2 by full-matrix least-squares calculations [70]. All non-H atoms have been refined anisotropically, whereas the H atoms have been treated with a riding model. Crystal data and structure refinement parameters for ***3*** are presented in Table 10.

Table 10. Crystallographic data for **4**

Empirical formula	$C_{16}H_{34}Ag_2CdN_8O_5$
Formula weight	746,65
Temperature [K]	296
Crystal size [mm]	0.1x0.2x0.3
Crystal system	Monoclinic
Space group	$P2_1$
a [Å]	9.243(5)
b [Å]	15.059(5)
c [Å]	10.416(5)
α = γ [°]	90.00
β [°]	111.367(5)
V [Å^3]	1350.2(11)
Z	2
ρcalcd. [g/cm^3]	1.837
μ [1/mm]	2.26
F(000)	736
θ range [°]	2.4 - 26.4
Index ranges	±11, ±18, ±13
Reflections collected	28586
Reflections observed(>2σ)	5510
Goodness-of-fit on F^2	1.064
R1 (all)	0.0340
wR2	0.0639

4.4. Biological Studies

4.4.1. Cell Culture

The anticancer potential of the complexes was investigated on cancerous HT29 (ATCC® HTB-38™), HeLa (ATCC® CCL-2™), and C6 cells (ATCC® CCL-107™) and nontumorigenic Vero cells (ATCC® CCL-81™). The cell lines were cultured in a cell medium (Dulbecco's modified eagle's) enriched with 10% (v/v) fetal bovine serum and 2% (v/v) Penicillin-Streptomycin (10,000 U/mL). First, old medium was removed out of the flask while cells had reached approximately 80% confluence. Next, cells were taken from the flasks surface using 4-5 mL of trypsin-EDTA solution and then subjected to centrifugation. Following, the cell pellet was suspended with 4 mL of DMEM working solution and was counted to obtain a final concentration of 5×10^4 cells/mL, and inoculated into wells (100 μL cells/well).

4.4.2. BrdU Cell Proliferation Assay (BCPA)

A cell suspension containing approximately 5×10^3 cells in 100 µL was seeded into the wells of 96-well culture plates. The cells were treated with complexes and control drug dissolved in sterile DMSO (max 0.5% of DMSO) at final concentrations of 0.25, 0.50, 1.00, 1.50, 2.00, 2.50, 3.75, and 5.00 µg/mL at 37°C with 5% CO_2 for overnight. The final volume of the wells was set to 200 µL by medium. Cell proliferation assay was evaluated by ELISA BrdU methods as described previously [34].

4.4.3. Calculation of % inhibition and IC_{50}

IC50 value is a concentration that inhibits half of the cells in vitro. The half maximal inhibitory concentration (IC50) of the test and control compounds was calculated using XLfit5 or excel spreadsheet and represent in µM at 95% confidence intervals. The proliferation assay results were expressed as the percent inhibition according to the following formula: % inhibition = [1 – (Absorbance of Treatments / Absorbance of DMSO) × 100].

4.4.4. Lactate Dehydrogenase (LDH) Cytotoxicity Assay

The cytotoxicity of the compounds on HeLa, C6, HT29, and Vero cells was determined through a Lactate Dehydrogenase Assay Kit according to the manufacturer's instructions. Approximately 5×10^3 cells in 100 µL were placed into 96-well plates as triplicates and treated with IC50 (µg/mL) concentrations of test compounds at 37°C with 5% CO_2 for 24 h. LDH activity was obtained by determining absorbance at 492 - 630 nm using a microplate reader.

4.4.5. Apoptotic potential by DNA laddering Assay

A DNA laddering activity of the test compounds was performed by using DNA laddering assay, it was described in accordance with the literature methods [71]. Briefly, 7.5 x 10^5 cells were placed into 25 cm^2 culture flasks, and treated with IC_{50} concentrations of test compounds at 37°C with 5% CO_2 for overnight. First, DNA-containing precipitate was extracted from digest with a 50 µL phosphate-citrate buffer, centrifuged at 1500 xg for 5 min, and then 40 µL supernatant was transferred to a micro centrifuge tube. Tween20 (5 µL) solution (0.25% in ddH_2O) and RNase A (5 µL) solution added to the supernatant, and then incubated at 37°C for 28 min. Next, proteinase K (5 µL) was added to each tube and re-incubated at 37°C for 8 min. Finally, DNA-containing precipitate of the micro centrifuge tube was added 2 µL of loading buffer and loaded

to 2% agarose gel containing 0.5 µg/mL ethidium bromide and electrophoresed at 200 mA for 40 min. After electrophoresis, DNA fragmentation on gels was imaged using UVP gel imagined system.

4.4.6. Apoptotic potential by TUNEL assay

The apoptosis was evaluated on HT29 cells using a TUNEL assay kit according to the manufacturer's protocol. The cells (30.000 /well) were seeded in a poly-L-lysine covered chamber slide and treated with the IC_{50} concentrations of test compounds at 37^{o}C for 24 hours. The assay was conducted guidance on the relevant method described by the literature [34]. Fluorescent signal was detected by a Leica fluorescent microscope (Leica DMIL LED fluo, Germany).

4.4.7. Cell migration assay

The migration feature of treated cells was conducted using the migration assay as described previously [34]. Briefly, the HeLa cells in equal number (3.5×10^4 cells in 70 µL DMEM) were plated into the two same reservoirs of the silicone pool. When cell density reaches to 80% confluence, the reservoir wall was throw and 2 mL of cell culture medium including IC30 concentrations of the compounds added, and then incubated at 37°C with 5% CO2. The movement of the cells into a wounded area was photographed until the gap covered by control cells.

4.4.8. DNA topoisomerase I inhibition assay

The anti-topoisomerase I activity of test compounds was found using topoisomerase I assay as described previously [34]. In brief, 0.25 µg/µL of plasmid pHOT1 DNA, 2 U recombinant human topoisomerase I enzyme, and IC50 concentrations of the compounds were added to reaction tube. The mixture was incubated at 37°C for 30 min and then the reaction terminated through adding stop solution. The mixture was loaded 1% agarose gel and electrophoresed for 60 min. DNA bands staining ethidium bromide photographed through a gel imaging system.

4.4.9. Cell imaging

Cells were plated in 96-well plates at a density of 5.000 cells per well and allowed 24 h. IC50 values of the test compounds were administered and morphology alters of the cells were screened by phase contrast microscopy for 24 h every 6 h. Images of control and test compounds

treated cells were photographed at the end of the process using a digital camera attached to an inverted microscope.

4.4.10. Immunohistochemistry

Immunohistochemistry (IHC) techniques were used to localize antigens with different expression levels following test compound treatment. Accordingly, HT29 and HeLa cells (15.000 cells/well) were seeded to µ-Slide with poly-L-lysine. The cells were subjected to IC50 concentrations of the test compounds and allowed incubation for 24 h. There was a negative control that had no test compounds. The IHC study of test compounds was evaluated using a Ventana IHC system according to manufacturer's directions. IHC was performed using Bcl-2 (mouse monoclonal, clone 124), CK7 (mouse monoclonal, clone OV-TL 12/30), CK20 (mouse monoclonal, clone Ks20.8), and P53 (mouse monoclonal, clone D07) on the VENTANA Bench-Mark XT System. The slides scores were rated as follows: 0 (<5% positive cells), 1 (5–24% positive cells), 2 (25-49% positive cells), 3 (>50% positive cells). The positive for relevant expression noted 2 or 3 while the negative stated 0 or 1.

4.4.11. Preparation of microorganisms and disc diffusion assay

A total of 10 microbial cultures belonging to ten bacterial species were used in this study. All the bacterial strains were cultured on Mueller–Hinton Broth (Merck) for 24 h at 36 ^{o}C. Disc-diffusion method was performed for antimicrobial tests [72] using 100 µL of suspension containing 10^8 CFU/mL of bacteria and 10^6 CFU/mL of yeast spread on Nutrient Agar (NA) and Potato Dextrose Agar (PDA) medium, respectively. The blank discs (Oxoid = 6 mm in diameter) were impregnated with 20 µL of the each substance (105 µg/disc) and placed on the inoculated agar. Solvent (KCN) was used as a negative control. Sulbactam (30 µg) + Cefoperazone (75 µg) (total 105 µg/disc) was used as a standard. The inoculated plates were incubated at 36 ^{o}C for 24 h. Antimicrobial activity was evaluated by measuring the zone of inhibition against the test organisms.

4.4.12. Microdilution assay

The minimal inhibition concentration (MIC) values were also studied for the microorganisms, which were determined to be sensitive to the substances tested in the disc-diffusion assay. İnocula of microorganisms were prepared using 12 h broth cultures and suspensions were adjusted to 0.5 McFarland standard turbidity. Each substance dissolved in 10 % dimethyl

sulfoxide (DMSO) was first diluted to the highest concentration (1000 µg/mL) to be tested. Then, serial twofold dilutions were made in a concentration range from 3.9–1000 µg/mL in 10-mL sterile test tubes containing nutrient broth. A prepared suspension of the standard microorganisms was added to each dilution in a 1:1 ratio. Growth (or its lack) of microorganisms was determined visually after incubation for 24 h at 36 ^{o}C. The lowest concentration at which there was no visible growth (turbidity) was taken as the MIC. This process was also repeated for the antibiotic. MIC values of the compounds against bacterial strains were determined on the basis of a micro-well dilution method [73].

4.4.13. Agar well diffusion bioassay for test fungi

Plant pathogenic fungal species *Alternaria solani*, *Rhizoctonia solani*, *Fusarium oxysporum* and *Sclerotinia sclerotiorum* were obtained from culture collection of Department of Plant Protection, Agricultural Faculty, Gaziosmanpasa University. They were cultured on potato dextrose agar (PDA) medium and then stored at 4 ºC until use. They were subcultured for 5-7 days in darkness at 25 ± 2 ºC by transferring from the stock cultures to PDA medium in Petri dishes. Antifungal effects of the compounds were tested by using agar well diffusion method with some modification [74]. Briefly, a 10 mL of PDA medium was poured into a 6-cm diameter sterile Petri dish. After solidification of the medium, the wells (5 mm diameter) were produced in the agar with sterile cork borer. Mycelial plugs (5-mm diameter) from the edge of cultured fungal colony were placed mycelial surface down on the medium at 30 mm apart from the well. The compounds **1**, **2** and **3** were diluted with 50 % DMSO solution to the final concentrations of 2.5, 5, 7.5, 10, 15, and 20 µg/mL then 20 µL of the diluted samples were pipetted into each well. All plates were then incubated in the dark at 25 ± 2 ºC for 7 days. After 7 days of incubation, diameters of the inhibition zones were measured(in mm). Three replicates were used for each treatment. 50 % DMSO was loaded in control plates as a negative control. Maneb (2.4 mg/mL) and cupper hydroxide (1.25 mg/mL) at manufacturer recommended rates were used as a positive control. The diameter of the inhibition zone was measured when the hyphae of the negative control extended to well. The rates of mycelial growth inhibition (GI %) was calculated by the following formula: GI % = dc-dt/dc*100 Where dc is mean colony diameter of control sets and dt is mean colony diameter of treatment sets [75]. Each test performed in triplicate.

4.4.14. DNA/BSA binding and gel electrophoresis studies

The binding constants (Kb) and the interaction of the compounds with Calf thymus-DNA (CT-DNA) were evaluated UV spectroscopy. A CT-DNA solution was prepared by dissolving 2.5 mg CT-DNA in 10.0 mL Tris–HCl buffer and it was immediately used. The concentration of CT-DNA was found spectrophotometrically with the aid of Ɛ value of 6600 M^{-1} cm^{-1} at 260 nm. After dissolving the CT-DNA fibers in Tris–HCl buffer, the purity of this solution was checked from the absorbance ratio A_{260}/A_{280}. The DNA was pure enough to use while the CT-DNA solution in the buffer displayed an A_{260}/A_{280} ratio of 1.83. Both compounds dissolving in DMSO re-diluted with Tris–HCl buffer to obtain 25 μM concentrations. Test compounds in the solutions were incubated at 20°C for about 30 min before measurements. The UV absorption spectrum data were conducted through unchanging the concentration of both compounds with increasing the CT–DNA concentrations (0-100 μM). Absorption spectra were recorded using 1-cm-path quartz cuvettes at room temperature [76].

To evaluate the interaction of the compounds with BSA UV spectroscopy was used. A BSA solution was prepared by dissolving 2.5 mg BSA in 10.0 mL in Tris–HCl buffer and it was immediately used. The scans of the BSA solutions (0-100 μM) with a fixed concentration of the complexes (25 μM) were screened in the wavelength range 250-320 nm.

Ethidium bromide (EB) displacement situation was carried out by tracking alters in the quenching severity of a constant concentration of EB-DNA solutions with test compounds (25–75 μM). The quenching severity of EB was screened using an excitation wavelength of 295 nm and the emission range was adjusted between 200 and 600 nm. The spectral data were examined with the Stern–Volmer equation, $I_0/I = 1 + K_{SV}$ [Q], where I_0 is the fluorescence severity in the absence of quencher, I is the fluorescence severity in the presence of quencher, K_{SV} is the Stern–Volmer quenching constant, and [Q] is the quencher concentration. K_{SV} can be calculated from the slope of the plot of I_0/I vs. $[DNA]$.

The restriction enzyme inhibition assay was conducted to evaluate both specific and nonspecific binding and enzyme inhibition by complexes. Supercoiled pTOLT (10 μM) plasmid DNA was incubated with the complexes (25 μM) and restriction enzymes *Kpn*I and *Bam*HI (2 units) at 37 °C in Tris–HCl/NaCl buffer (50/18 mM, pH 7.2) for 4 h. The digestion products were observed by using 1.5% (wt/vol) agarose gels with ethidium bromide.

4.4.15. Statistical Analysis

Statistical significance of differences were determined by the one-way analyses of variance (one-way ANOVA) followed by Tukey test. Data did not show homogeneity variances that

were analyzed by the non-parametric Kruskal-Wallis test. The SPSS for Windows computer program was used for statistical analyses. Results are reported as mean values ± SEM of three independent assays and differences between groups were considered to be significant at $P<0.05$. Inhibition zone data was analyzed using POLO-PC Probit [77] to estimate lethal concentration 50, and 90 values (LC50, and 90) and the regression line slope.

Acknowledgments

The authors thank the Scientific and Technical Research Council of Turkey (TUBİTAK, Grant TBAG-112T696; COST Action CM 2515) and the Gaziosmanpaşa University Research Foundation (Grant 2011/32) for financial support. Also, the authors are grateful to Professor Yusuf Yerli for EPR and magnetic measurements: The University of Yildiz Technical.

Appendix A. Supplementary data

X-ray crystallographic files in CIF format for **4**, crystallographic data for the structure reported here has been deposited with the Cambridge Crystallographic Data Centre as supplementary data, CCDC Nos. 1043613. Copies of the data can be obtained through application to CCDC, 12 Union Road, Cambridge CB2 1EZ, UK. (Fax: +44 1223 336033 or e-mail: deposit@ccdc.cam.ac.uk or at http://www.ccdc.cam.ac.uk).

References

[1] C. Avendaño, J.C. Menéndez, Medicinal Chemistry of Anticancer Drugs. 1st ed. Amsterdam, the Netherlands: Elsevier BV, 2008.

[2] B. Thati, A. Noble, B.S. Creaven, M. Walsh, M. McCann, K. Kavanagh, M. Devereux, D.A. Egan, Cancer Lett. 248 (2007) 321–331. *http://dx.doi.org/10.1016/j.canlet.2006.08.009*

[3] H.L. Zhu, X.M. Zhang, X.Y. Liu, X.J. Wang, G.F. Liu, A. Usman, H.K. Fun, Inorg. Chem. Commun. 6 (2003) 1113–1116. *http://dx.doi.org/10.1016/S1387-7003(03)00205-3*

[4] J.J. Liu, P. Galettis, A. Farr, L. Maharaj, H. Samarasinha, A.C. McGechan, B.C. Baguley, R.J. Bowen, S.J. Berners-Price, M.J. McKeage, J. Inorg. Biochem. 102 (2008) 303–310. *http://dx.doi.org/10.1016/j.jinorgbio.2007.09.003*

[5] P.C. Zachariadis, S.K. Hadjikakou, N. Hadjiliadis, S. Skoulika, A. Michaelides, Balzarini, E. De Clercq, Eur. J. Inorg. Chem. 7 (2004) 1420–1426. *http://dx.doi.org/ 10.1002/ejic.200300672*

[6] S.E.H. Etaiw, A.S. Sultan, A.S. Badr El-din, Eur. J. Med. Chem. 46 (2011) 5370–5378. *http://dx.doi.org/10.1016/j.ejmech.2011.08.041*

[7] S. Tanase, F. Tuna, P. Guionneau, T. Maris, G. Rombaut, C. Mathonière, M. Andruh, O. Kahn, J-P. Sutter, Inorg. Chem., 2003, 42(5), 1625–1631. *DOI: 10.1021/ic025990z*

[8] K. Tomono, Y. Tsunobuchi, K. Nakabayashi and S-i. Ohkoshi, Inorg. Chem., 49 (2010) 1298–1300.
[9] X.-Q. Wei, K. Qian, H.-Y. Wei, X.-Y. Wang, Inorg.Chem. 55 (2016) 5107−5109. DOI:10.1021/acs.inorgchem.6b00787
[10] J. Černák, M. Orendáč, I. Potočňák, J. Chomič, A. Orendáčová, J. Skoršepa, A. Feher, Coord. Chem. Rev. 224 (2002) 51-66. http://doi.org/10.1016/S0010-8545(01)00375-7
[11] M. C. Muñoz, J. A. Real, Coord. Chem. Rev. 255 (2011) 2068– 2093. http://dx.doi.org/10.1016/j.ccr.2011.02.004
[12] Ş. A. Korkmaz, A. Karadağ, Y. Yerli, M. S. Soylu, New J. Chem. 38 (2014) 54020–5410. http://doi.org/10.1039/c4nj00737a
[13] M. Vavra, I. Potocnák, M. Dušek, Inorganica Chimica Acta 409 (2014) 441–448 http://dx.doi.org/10.1016/j.ica.2013.09.016
[14] Ş. A. Korkmaz, A. Karadağ, A. Aydın, Y. Yerli, M. S. Soylu, Inorg. Chim. Acta 453 (2016) 154–168. http://doi.org/10.1039/c4nj00737a
[15] J. R. Stork, D. Rios, D. Pham, V. Bicocca, M. M. Olmstead, A. L. Balch, Inorg. Chem. 44 (2005) 3466–3472. http://doi.org/10.1021/ic048333a
[16] A. M. Madalan, N. Avarvari, M. Andruh, Crystal Growth & Design, 6(7) (2006) 1671–1675. http://doi.org/10.1021/cg060131x
[17] A. Karadağ, A. Aydın, S. Dede, Ş. Tekin, Y. Yanar, B. H. Çadırcı, M. S. Soylu, Ö. Andaç, New J. Chem. 39 (2015) 8136–8152. http://doi.org/ 10.1039/c5nj01108f
[18] T. Soma, T. Iwamoto, Chem. Lett. 4 (1994) 821–824. http://dx.doi.org/10.1246/cl.1994.821.
[19] J. Černák, F. Ge´rard, J. Chomič, Acta. Cryst. C49 (1993) 1294-1296. http://doi.org/10.1107/S010827019300037X
[20] T. Soma, T. Iwamoto, Inorg. Chem. 35 (1996) 1849–1856. http://dx.doi.org/10.1021/ic950629q.
[21] J.J. Černák, K.A. Abboud, J. Chomič, M.W. Meisel, M. Orendáč, A. Orendáčová, A. Feher, Inorg. Chim. Acta. 311 (2000) 126–132. http://doi.org/10.1016/S0020-1693(00)00327-3.
[22] K.J. Range, S. Kühnel, M. Zabel, Acta Crystallogr. Sect. C Cryst. Struct. Commun. C45 (1989) 1419–1420. http://dx.doi.org/10.1107/S010827018900613X.
[23] C. Kappenstein, A. Ouali, M. Guerin, J. Černák, J. Chomič, Inorg. Chim. Acta. 147 (1988) 189. http://dx.doi.org/10.1016/S0020-1693(00)83370-8
[24] C. Y. Chen, J. Y. Zeng, H. M. Lee, Inorg. Chim. Acta 360 (2007) 21–30. http://dx.doi.org/10.1016/j.ica.2006.06.013
[25] Z.-H. Wang, D.-F. Wang, T. Zhang, R.-B. Huang, L.-S. Zheng, CrystEngComm, 16 (2014) 5028–5039. http://dx.doi.org/10.1039/c4ce00072b
[26] D. Yadav, R. K. Siwatch, G. Mukherjee, G. Rajaraman, S. Nagendran, Inorg. Chem. 53 (2014) 10054−10059. dx.doi.org/10.1021/ic5008389
[27] M. Salavati-Niasari, Polyhedron 24 (2005) 1405-1409. http://doi.org/10.1016/j.poly.2005.03.060
[28] M. Salavati-Niasari, M. Bazarganipour, Inorg. Chem. Commun. 9 (2006) 332-336. http://doi.org/10.1016/j.inoche.2005.12.011
[29] A. Şenocak, A. Karadağ, Y. Yerli, Ö. Andaç, E. Şahin, J. Inorg. Organomet. Polym.

Mater. 20 (2010) 628–635.
http://doi.org/10.1007/s10904-010-9361-x
[30] A. Karadağ, A. K. Gözüaçık, V.T. Yılmaz, Y. Yerli, E. Şahin, Polyhedron 78 (2014) 24-30.
http://doi.org/10.1016/j.poly.2014.03.056
[31] A. Şenocak, A. Karadağ, M.S. Soylu, Ö. Andaç, New J Chem. 39 (2015), 3675-3686
http://doi.org/10.1039/c5nj00071h
[32] H. Zhang, J. Cai, X.-L. Feng, T. Li, X.-Y. Li, L.-N. Ji, Inorg. Chem. Commun. 5 (2002) 637–641.
http://doi.org/10.1016/S1387-7003(02)00514-2
[33] L. Triščíková, J. Chomič, K. A. Abboud, J.-H. Park, M. W. Meisel, J. Černák, Inorganica Chim. Acta 357 (2004) 2763–2768.
http://doi.org/10.1016/j.ica.2004.02.008
[34] N. Korkmaz, A. Karadağ, A. Aydın, Y. Yanar, İ. Karaman, Ş. Tekin, New J. Chem. 38 (2014) 4760–4773.
http://doi.org/10.1039/C4NJ00851K
[35] J.K. Burdett, R. Hoffmann, R.C. Fay, Inorg. Chem. 17 (1978) 2553-2567.
http://doi.org/10.1021/ic50187a041
[36] E.L. Muetterties, C.M. Wright, Q. Rev. Chem. Soc. 21 (1967) 109-19
http://doi.org/10.1039/qr9672100109
[37] J. Xu, E. Radkov, M. Ziegler, K.N. Raymond, Inorg. Chem. 39 (2000) 4156-416
http://doi.org/10.1021/ic000063i
[38] R.J. Dudley, B.J. Hathaway, J. Chem. Soc. A, 12 (1970) 2799–280
http://doi.org/10.1039/J19700002799
[39] E. Di Mauro, S. Mara Domiciano, J. Phys. Chem. Solids, 60 (1999) 1849–185
http://doi.org/10.1016/S0022-3697(99)00198-5
[40] Y. Yerli, S. Kazan, O. Yalçın, B. Aktaş, Spectrochim. Acta Part A Mol. Biomol. Spectrosc. 64 (2006) 642–645.
http://doi.org/10.1016/j.saa.2005.07.068
[41] Y. Yerli, F. Köksal, A. Karadag, Solid State Sci., 5 (2003) 1319–132
http://doi.org/10.1016/S1293-2558(03)00186-9
[42] B. Karabulut, R. Tapramaz, A. Karadağ, Appl. Magn. Reson., 35 (2008) 239–245.
http://doi.org/10.1007/s00723-008-0158-9
[43] A. Şenocak, A. Karadağ, E. Şahin Y. Yerli, J Inorg. Organomet. Polym., 21 (2011):438–449.
http://dx.doi.org/10.1007/s10904-011-9466-x
[44] A. Karadağ, Ş. A. Korkmaz, Ö. Andaç, Y.Yerli, Y. Topçu, J. Coord. Chem. 65(10) (2012) 1685–1699.
http://dx.doi.org/10.1080/00958972.2012.678337
[45] A. Şenocak, A. Karadağ, Y. Yerli, N. Gürbüz, İ. Özdemir, E. Şahin, Polyhedron 49 (2013) 50–60.
http://dx.doi.org/10.1016/j.poly.2012.09.030
[46] Ş. A. Korkmaz, A. Karadağ, N. Korkmaz, Ö. Andaç, N. Gürbüz, İ. Özdemir, R. Topkaya, J. Coord. Chem. 66(17) (2013) 3072–3091.
http://dx.doi.org/10.1080/00958972.2013.820827
[47] N. Korkmaz, Supervisor: A. Karadağ, Synthesis, Characterization, Antibacterial and Anticancer Activities of Coordination Compounds Containing Dicyanidoargentat(I), PhD thesis, University of Gaziosmanpasa, Turkey, 2014.
[48] M. Vavra, I. Potocnák, M. Marhefková, R. Boca, L. Dlhán Polyhedron 48 (2012) 227–236.
http://dx.doi.org/10.1016/j.poly.2012.08.070
[49] I. Bhowmick, D. T. Harris, P. Dechambenoit, E. A. Hillard, C. Pichon, Ie-R. Jeon, R. Clérac, Sci. China Chem. 55(6) (2012) 1004–1011.
doi: 10.1007/s11426-012-4592-z
[50] A. Aydın, N. Korkmaz, Ş. Tekin, A. Karadağ, Turkish J. Biol. 38 (2014) 948–955.

http://doi.org/10.3906/biy-1405-68
[51] A. Aydın, A. Karadağ, Ş. Tekin, N. Korkmaz, A. Özdemir, Turkish J. Chem. 39 (2015) 532–549. http://doi.org/10.3906/kim-1412-13
[52] A. Aydın, A. Karadağ, Ş. Tekin, N. Korkmaz, A. Özdemir, Turkish J. Chem. 39 (2015) 532–549. http://doi.org/10.3906/kim-1412-13
[53] A. Aydın, A. Karadağ, Ş. Tekin, N. Korkmaz, A. Özdemir, Turkish J. Chem. 39 (2015) 532–549. http://doi.org/10.3906/kim-1412-13
[54] A. Karadağ, A. Aydın, S. Dede, Ş. Tekin, Y. Yanar, B. H. Çadırcı, M. S. Soylu, Ö. Andaç, New J. Chem. 39 (2015) 8136–8152. http://doi.org/10.1039/C5NJ01108F
[55] A. Karadag, A. Aydın, A. Özdemir, Ş. Tekin, J. Biotechnol. 185 (2014) S105. http://doi.org/10.1016/j.jbiotec.2014.07.358
[56] S. Tekin, A. Aydın, S. Dede, A. Karadağ, J. Biotechnol. 185 (2014) S28–S29. http://doi.org/10.1016/j.jbiotec.2014.07.096
[57] M.A. Iqbal, R.A. Haque, S.F. Nasri, A.A. Majid, M.B.K. Ahamed, E. Farsi, T. Fatima, Chem. Cent. J. 7 (2013) 27. http://dx.doi.org/10.1186/1752-153X-7-27
[58] R. Govender, A. Phulukdaree, R.M. Gengan, K. Anand, A.A. Chuturgoon, J. Nanobiotechnology 11 (2013) 5. http://dx.doi.org/10.1186/1477-3155-11-5
[59] V. Gandin, M. Pellei, M. Marinelli, C. Marzano, A. Dolmella, M. Giorgetti, C. Santini, J. Inorg. Biochem. 129 (2013) 135–144. http://dx.doi.org/10.1016/j.jinorgbio.2013.09.011
[60] H. Zetty Zulikha, R.A. Haque, S. Budagumpi, A.M.S. Abdul Majid, Inorganica Chim. Acta 411 (2014) 40–47. http://dx.doi.org/10.1016/j.ica.2013.11.011
[61] J.J. Champoux, Annu. Rev. Biochem. 70 (2001) 369–413. http://dx.doi.org/10.1146/ annurev.biochem.70.1.369
[62] K.A. Ali, M.M. Abd-Elzaher, K. Mahmoud, Int. J. Med. Chem. 2013 (2013) 1– http://dx.doi.org/10.1155/2013/256836
[63] C. Pettinari, F. Marchetti, G. Lupidi, L. Quassinti, M. Bramucci, D. Petrelli, L.A. Vitali, M.F.C. Guedes da Silva, L.M.D.R.S. Martins, P. Smoleński, A.J.L. Pombeiro, Inorg. Chem. 50 (2011) 11173–11183. http://dx.doi.org/10.1021/ic201714c
[64] C.N. Banti, S.K. Hadjikakou, Metallomics 5 (2013) 569–596. http://dx.doi.org/ 10.1039/C3MT00046J
[65] X. Wu, J.C. Yalowich, B.B. Hasinoff, J. Inorg. Biochem. 6 (2011) 833–88 http://dx.doi.org/10.1016/j.jinorgbio.2011.02.007
[66] I.H. Hall, M.C. Miller, D.X. West, Met. Based Drugs 2 (1997) 89–95. http://dx.doi.org/10.1155/MBD.1997.89
[67] R. Prabhakaran, R. Sivasamy, J. Angayarkanni, R. Huang, P. Kalaivani, R. Karvembu, F, Dallemer, K, Natarajan, Inorg. Chim. Acta. 374 (2011) 647–653. http://dx.doi.org/10.1016/j.ica.2011.03.020.
[68] S.R. Satapathy, P. Mohapatra, R. Preet, D. Das, B. Sarkar, T. Choudhuri, M.D. Wyatt, C. N. Kundu, Nanomedicine 8 (2013) 1307–1322. http://dx.doi.org/10.2217/nnm.12.176
[69] Rigaku Crystal-Clear, Version 1.3.6; Rigaku American Corporation 9009 New Trails Drive, The Woodlands, TX 77381-5209, USA, 2005.
[70] G.M. Sheldrick, SHELXS97 and SHELXL97, University of Gottingen, Germany, 1997.
[71] J.P. Gong, F. Traganos, Z. Darzynkiewicz, Anal. Biochem. 218 (1994) 314–319. http://doi.org/10.1006/abio.1994.1184

[72] P.R. Murray, E.J. Baron, M.A. Pfaller, F. C. Tenover, R. H. Yolke, Manual of Clinical Microbiology, ASM, Washington, DC, vol. 6, 1995.
[73] J.R. Zgoda, J.R. Porter, Pharm. Biol. 39 (2001) 221–225. *http://doi.org/10.1076/phbi. 39.3.221.5934*
[74] L. Boyanova, G. Gergova, R. Nikolov, S. Derejian, E. Lazarova, N. Katsarov, I. Mitov, Z. Krastev, J. Med. Microbiol. 54 (2005) 481–483. *http://doi.org/10.1099/jmm.0.45880-0*
[75] P. Tripathi, N.K. Dubey, A.K. Shukla, World J. Microbiol. Biotechnol. 24 (2008) 39–46. *http://doi.org/10.1007/s11274-007-9435-2*
[76] M. Sirajuddin, A. Badshah, J. Photochem. Photobiol. B 124 (2013) 1–19. *http://dx.doi.org/10.1016/j.jphotobiol.2013.03.013*
[77] Leora Software, 1119 Shattuck Avenue, Berkeley, CA, 1994.

Graphical abstract

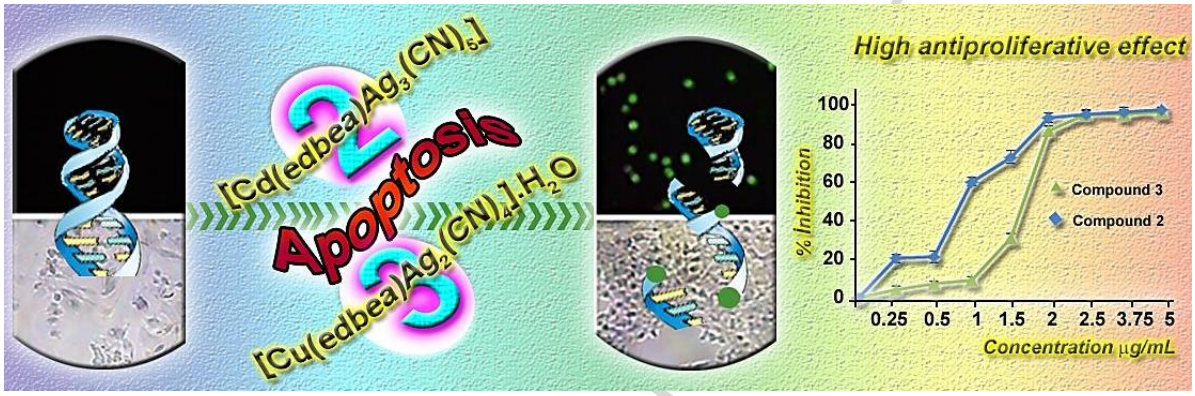

The dicyanidoargentate(I)-based complexes are originally synthesized, potential anticancer compounds with antibacterial and antifungal activity *in vitro* also. The tested complexes are exterior due to possessing highly potential biological activities together in each complexes.

Highlights

- [Cd(*edbea*)$Ag_3(CN)_5$].H_2O (**3**) is a patented compound at national level (TR 2012 08885 B).
- The crystal structures of [Cd(*edbea*)$_2$][$Ag(CN)_2$]$_2$.H_2O (**4**) was determined.
- Interaction of CT-DNA/BSA with these compounds were spectroscopically examined.
- We used DNA laddering, TUNEL, topoisomerase I, cell migration and immunohistochemical assays.
- Antibacterial and antifungal activity tests were performed.